Comparative Study of Converter-fed Reluctance Synchronous- and Induction Motor System Efficiencies

by

Andrew Thomas Loubser,

Thesis presented in partial fulfilment of the requirements for the degree of Master of Electrical Engineering in the Faculty of Engineering at Stellenbosch University

Supervisor: Prof. M.J. Kamper

December 2017

Declaration

By submitting this thesis electronically, I declare that the entirety of the work contained therein is my own, original work, that I am the sole author thereof (save to the extent explicitly otherwise stated), that reproduction and publication thereof by Stellenbosch University will not infringe any third party rights and that I have not previously in its entirety or in part submitted it for obtaining any qualification.

Date: December 2017 .....

Abstract

Comparative Study of Converter-fed Reluctance Synchronous- and Induction Motor System Efficiencies

A.T. Loubser (13734849)

Department of Electrical and Electronic Engineering,
University of Stellenbosch,
Private Bag X1, 7602 Matieland, South Africa.

Thesis: MEng (Electrical)

September 2017

Energy efficiency in electric motor driven systems is becoming an increasingly important topic of study. As such, this thesis deals with the comparison of the drive system efficiencies of a reluctance synchronous motor (RSM) and an induction motor (IM) based on international standards for efficiency classification. It approaches this goal through the complete design optimisation of a 5.5 kW, 50 Hz, 4-pole, 3-phase reluctance synchronous motor (RSM) with inverter losses taken into account. Analytical calculations, based in part on finite element analysis, are used to determine the drive system efficiency. A simulation model of the RSM is developed and used to generate the optimised design. Optimisation results show that by maximising drive system efficiency, the motor's power factor is automatically improved to reduce inverter losses. The optimised RSM is built and tested alongside the IM based on the international standards, and comparisons are made regarding the performance of both motors. The results show that the RSM drive system is able to outperform the IM by a significant degree at this power level. Further conclusions regarding the optimisation model and the performance of the RSM are made, and recommendations for future studies are proposed.

Uittreksel

Vergelykende Studie van die Stelsel Benuttingsgraad van Omsetter-gevoerde Sinchroon Reluktansie- en Induksie Motors

A.T. Loubser (13734849)

Departement Elektriese en Elektroniese Ingenieurswese,
Universiteit van Stellenbosch,
Privaatsak X1,7602 Matieland, Suid Afrika.

Tesis: MIng (Elektries)

September 2017

Die benuttingsgraad van elektriese motoraangedrewe stelsels word alhoemeer 'n belangrike onderwerp. As sulks handel hierdie tesis oor die vergelyking van die stelsel benuttingsgraad van 'n sinchroon reluktansiemotor (RSM) en 'n induksiemotor (IM), gebaseer op internasionale standaarde. Dit benader hierdie doel deur middel van die volledige ontwerpsoptimeering van 'n 5.5 kW, 50 Hz, 4-pool, 3-fase sinchroon reluktansiemotor, met omsetter verliese in ag geneem. Analitiese berekeninge, gedeelteliks gebaseer op eindige element metodes, word gebruik om die stelsel se benuttingsgraad vas te stel. 'n Simulasie model van die RSM is ontwikkel en gebruik om 'n geoptimeerde ontwerp te genereer. Die resultate van die optimeering wys dat deur die stelsel benuttingsgraad te maksimeer, word die arbeidsfaktor van die motor indirek geoptimeer om omsetterverliese te verminder. Die ge-optimeerde RSM is gebou en tesame die IM getoets, gebaseer op die internationale standaarde, en vergelykings word gemaak aangaande die vermoë van beide motors. Die resultate wys dat die RSM stelsel baie meer effektief as die IM stelsel is op hierdie drywingsvlak. Verdere afleidings aangaande die optimeeringsmodel en die werking van die RSM word gemaak, en navorsingprojekte word aanbeveel.

Acknowledgements

I would like to acknowledge and thank the following people for their various contributions:

My wife, Monda. For all the patience and support she has given me over the years. I couldn't have done this without her.

My parents, Andrew and Anna Loubser. Their continuous support throughout the years has allowed me to take the time that I needed to reach my goals. Their gentle prodding and shared insights helped to keep me moving forward when it wasn't clear what I was moving towards. There aren't sufficient words to fully express the extent of my gratitude to them.

Prof. M.J. Kamper. My supervisor and my mentor. His support extended far beyond what could be expected from any supervisor. He helped me see the value in my work and gave me the opportunity to present that work to some of the greatest minds in our field. I will always be deeply grateful for everything he has done for me and for the opportunity I have been given to learn from him.

Dr. Stiaan Gerber, the master (developer) of SEMFEM. For answering hundreds of questions with total patience and helping me to find insight where insight was lacking. Also for shooting the breeze from time to time or shooting each other in the lunch-time game.

Eddy and Albert, for the conversations and assistance around the RSM that helped me plot the way forward in my work at various turns. Reaching the end-goal of my thesis would have been a little more difficult and a little less entertaining without them.

Josh Mitchell, for the use of his current control algorithm as well as the many conversations around the shared interest of music.

Dedications

I dedicate this thesis and the work herein to my wife, Monda, for her love, support, eternal patience and unwavering belief in me that kept me going when no end seemed in sight. She is the source from which I draw all motivation and inspiration. She is my light. She is my strength.

Publications

A. T. Loubser and M. J. Kamper, "Design optimisation of reluctance synchronous machine for drive system efficiency," 2015 IEEE Workshop on Electrical Machines Design, Control and Diagnosis (WEMDCD), Torino, 2015, pp. 60-65. Available at http://ieeexplore.ieee.org

Contents

List of Figures

List of Tables

Nomenclature

Abbreviations

2D	Two Dimensional
3D	Three Dimensional
CDM	Complete Drive Module
EMF	Electro Motive Force
EPA	Extended Product Approach
FEM	Finite Element Method
FPGA	Field Programmable Gate Array
IM	Induction Motor
IEC	International Electrotechnical Commission
IEP	Integrated Energy Plan
IGBT	Insulated Gate Bipolar Transistor
LV	Low Voltage
MEPS	Minimum Energy Performance Standards
MTPA	Maximum Torque Per Ampere
NEES	National Energy Efficiency Strategy
PDS	Power Drive System
PWM	Pulse Width Modulation
RSM	Reluctance Synchronous Motor
SABS	South African Bureau of Standards
SADoE	South African Department of Energy
SANS	South African National Standards
RCDM	Reference Complete Drive Module
RM	Reference Motor

RPDS	Reference Power Drive System
TS	Technical Specification
VSD	Variable Speed Drive

Symbols

a	Shaft Radius	[m]
c, x, y	Steinmetz Coëfficients	[ ]
d_i	Stator Inner Diameter	[m]
f_1	Fundamental Supply Frequency	[Hz]
f_s	Inverter Supply Frequency	[Hz]
k_{exp}	Core Loss Experience Factor	[ ]
k_d	Winding Distribution Factor	[ ]
$k_{e(2)}$	2-Pole Pair End-Winding Factor	[ ]
$k_{p(2)}$	End-Winding Coil Pitch Factor for Elliptical Coil Shapes	[ ]
l	Stack Length	[m]
l_e	Average Length of Winding Ends	[m]
m	Number of Phases	[ ]
m_a	Modulation Index	[ ]
n_a	Number of Parallel Winding Circuits	[ ]
p	Number of Pole Pairs	[ ]
r	Polar Distance	[m]
r_{HL}	Harmonic Loss Efficiency De-Rating Factor	[ ]
t_{off}	IGBT Switch-Off Time	[s]
t_{on}	IGBT Switch-On Time	[s]
z	Number of Conductors per Stator Slot	[ ]
λ_d, λ_q	dq Flux Linkages	[Wb]
θ	Polar Angle	[rad]
ω_e	Angular Speed of Electrical Reference Frame	[rad/s]
ω_m	Angular Shaft Speed	[rad/s]
ρ_t	Resistivity of Copper at Temperature t_c	[Ω m]
ϕ	Power Factor Angle	[rad]

η_{MUT}	Efficiency of Motor Under Test	[%]
η_n	New Nominal Efficiency Limit	[%]
η_{ref}	Reference Nominal Efficiency Limit	[%]
η_{inv}	Inverter Efficiency	[%]
η_{DS}	Drive System Efficiency	[%]
A_{Cu}	Active Copper Area per Stator Slot	[mm^2]
B_{tooth}	Maximum Flux Density in Stator Teeth	[T]
B_{yoke}	Maximum Flux Density in Stator Yoke	[T]
C	Characteristic Constant of Field Line	[ ]
E_d, E_q	dq Speed Voltages	[V]
E_a	Phase Voltage	[V_{rms}]
I_o	Peak Phase Current	[A]
I_d, I_q	dq Assigned Currents	[A]
I_{d1}, I_{q1}	Derived dq Supply Currents	[A]
I_{s1}	Derived Phase Current	[A_{rms}]
L_e	End-Winding Leakage Inductance	[H]
M_{tooth}	Total Mass of Stator Teeth	[kg]
M_{yoke}	Total Mass of Stator Yoke	[kg]
R_c	Core Resistance	[Ω]
R_s	Per Phase Stator Copper Resistance	[Ω]
T_{avg}	Average Torque	[Nm]
T_{max}	Maximum Torque	[Nm]
T_{min}	Minimum Torque	[Nm]
T_{rip}	Torque Ripple	[Nm]
P_{add}	Assigned Additional (Stray) Load Losses	[W]
P_{dev}	Developed Power	[W]
P_{cond}	IGBT Conduction Losses	[W]
P_{core}	Iron Core Losses	[W]
P_{diode}	IGBT Reverse Diode Conduction Losses	[W]
P_{inv}	Inverter Losses	[W]
P_{in}	Input Power	[W]

P_{out}	Power	[W]
P_{switch}	IGBT Switching Losses	[W]
Pf	Power Factor	[ ]
V_2	Shape Factor for Elliptical Double-Layer Winding Ends	[ ]
V_d, V_q	Derived dq Supply Voltages	[V]
V_{diode}	Diode Forward Voltage	[V]
V_{DC}	DC-Link Voltage	[V]
V_{on}	IGBT Forward Conduction Voltage	[V]
V_{s1}	Derived Supply Phase Voltage	[V_{rms}]
W	Number of Turns in Series per Phase	[ ]

Chapter 1

Introduction

1.1 Background

Increasing energy demands and supply limitations have resulted in most developed countries publishing minimum energy performance standards (MEPS), and progressively tightening them, in an effort to promote efficient energy usage. Furthermore, institutions like the International Electrotechnical Commission (IEC), the European Committee for Electrotechnical Standardization (CENELEC), and many others, have over the last 10 years published and maintained various standards with the goal of harmonizing efficiency determination and classification across the world. Many of these standards and regulations apply to electric motors as these systems consume the largest part of generated electricity in European industry. In South Africa the highest consumer of electricity in industry is process heating, but this hasn't stopped the South African Bureau of Standards (SABS) of publishing its own efficiency standards for electric motors based heavily on the published work of the IEC. The conclusion that can be drawn from this, and many other trends regarding the reduction of energy wastage, is that efficient electricity consumption is fast becoming a priority within the global industrial context.

The most widely used electric motor in the industry is the induction motor (IM), because of the ease with which it can be installed and operated directly on-line without the need for a converter. Also, with the largest cost associated with running an electric motor coming from its energy consumption, and with electricity prices climbing, it is no wonder that industries are looking for more efficient ways of driving their processes.

It is a long established fact that the use of a variable speed drive (VSD) can lead to large energy savings in any application where variable speed or torque is required [2]. This means that electric motor technologies that require a VSD to operate effectively, such as the reluctance synchronous motor (RSM), become attractive alternatives to the IM [3].

The RSM has re-emerged as a focus of study in recent decades due to its potential for high torque density and lower losses, giving it the potential to reach higher efficiency levels than what is attainable by the IM. Many researchers have compared these characteristics of the RSM to those of the IM at various power levels and for different application, or focused on improving one aspect of the RSM, such as minimising torque ripple through flux barrier design [4; 5; 6]. However, the RSM's relatively low power factor is one of its primary drawbacks. This is important as the lower power factor of the RSM relative to the IM leads to increased losses in the VSD, which could negate the efficiency advantage of the RSM.

With all this taken into consideration, it would be of interest to investigate the effect inclusion of the inverter losses would have on the design optimisation of the RSM. Additionally, a comparison of the variable speed/torque efficiency performance of a RSM drive system to that of an IM drive system would assist in establishing the viability of considering the RSM in these applications. To the author's knowledge no studies have been conducted hitherto on the optimum design of the RSM while taking the efficiency of the VSD into account.

1.2 Research Question

Does the reluctance synchronous motor maintain its efficiency advantage over the induction motor, for variable speed applications at a power level of 5.5 kW, when inverter losses are taken into account?

1.3 Research Aims and Objectives

It is the intent of the author to determine, within reasonable certainty, how the efficiency of a RSM based Power Drive System (PDS) compares to that of

an IM based PDS. The goal may be achieved through the completion of the following steps:

1. Determine which performance parameters to base the comparison on.
2. Design and optimise a RSM PDS model using semi-analytical methods.
3. Build the RSM PDS and assemble it together with the IM PDS to determine their respective performance characteristics.
4. Analyse and compare the performance of the two systems.

1.4 Scope/Limitations and Assumptions

- The study encompasses only the performance characteristics of the RSM PDS and IM PDS as compared to each other. No comparison is made with regard to any other electrical drive system.
- The research pertains specifically to variable speed/torque applications. Hence, testing the IM in online mode is outside the scope of this study as it is only applicable to single speed applications.
- It is known in practice that there exists a power level where the IM regains the efficiency advantage over the RSM. The author makes no attempt to determine exactly what this power level is with regards to the chosen application. Thus, specific results from this research isn't applicable to other power levels and generalised results are only applicable in an unknown bracket of power levels.
- An oversight made by the author in the design of the RSM required the RSM to be tested for a rated voltage of 390 V. While this doesn't fully negate any comparison made with the IM, the possible effect this may have on the final results should be considered when the comparisons are made.

1.5 Significance of Research

In the global context, efficient energy usage is quickly becoming one of the primary topics of concern. Hence, the research conducted as part of this thesis is applicable to any industry where electric motor driven systems make up a significant part of its processes. As the approach of including inverter losses in the design optimisation hasn't been used before, to the best knowledge of

the author, any conclusion that may be drawn from it could be used to further improve future design optimisations.

1.6 Thesis Layout

The purpose of Chapter 1 has been to provide the context wherein the research is conducted. The rest of the thesis is laid out as follows:

- Chapter 2 expands on the context already given in Chapter 1 by providing information on current regulations and standards pertaining to energy efficiency in motor driven systems. It then goes further by giving the reader a look at the current state of some of the knowledge surrounding the RSM in literature.
- Chapter 3 deals with the design choices for the RSM and with the analytical calculation of the various performance characteristics. It also provides the basis on which the comparisons between the RSM and IM are made.
- Chapter 4 explains the process by which the RSM design is optimised and gives the results of the optimisation. Preliminary conclusions are made regarding the inclusion of inverter losses in the process. The chapter ends with the validation of the simulation model and the optimised design by two methods.
- Chapter 5 provides more detail on the means by which the experiments are carried out and the performance of the RSM and IM drive systems are measured. The results of the experiments are given and comparisons are made between the system efficiencies of the RSM and IM. Further conclusions are also drawn regarding the accuracy of the optimisation model.
- Chapter 6 is where the conclusions of the study are summarised and recommendations for future studies are made.

Chapter 2

Literature Review

2.1 Regulations, Standards and Classifications

It is intended that the results given in this thesis be applicable to industry both in South Africa and abroad. To achieve that goal an understanding of current and future regulations, and the standards they are based on, is required.

2.1.1 Energy Efficiency Regulations

The South African Department of Energy (SADoE),which under the National Energy Act of 2008 is the government body responsible for all energy related regulations in the country, has been making efforts to promote efficient energy usage in the country through the Integrated Energy Plan (IEP) of 2016 [7] and the National Energy Efficiency Strategy (NEES) [8]. However, while the IEP gives a by sector analysis of current energy trends in South Africa and the NEES sets efficiency targets for each sector, the SADoE currently has no Minimum Energy Performance Standard (MEPS) with regards to electric motors.

Europe has a MEPS for electric motors which it has been progressively tightening since the publishing of legislation in 2009. As it stands now, since the start of 2017 it is mandatory that all new three-phase induction motors, in the power range 0.75 kW to 375 kW that are intended for direct-on-line operation, have a minimum efficiency classification of IE3 (premium efficiency)[9; 1]. The regulations still allow for any motors that are meant to be used with a VSD to

have at least an IE2 (high efficiency) classification, in recognition of the energy savings potential in these applications.

The EU MEPS is primarily based on the IEC standards that deal with the classification (IEC 60034-30-1) and testing (IEC 60034-2-1) of electric motor efficiencies. However, these standards and regulations only deal with motors meant for direct-on-line operation and so the EU is in the process of updating its regulations. They intend to include an extended product approach (EPA) by 2018, based on the CENELEC standards EN 50598-1&2, for low voltage (LV) motors and drive systems in the power range 0.12 kW to 1000 kW [1].

2.1.2 Efficiency Standards and Classifications

Despite there not being any MEPS for electric motors in South Africa, the South African Bureau of Standards (SABS) has published various South African National Standards (SANS) with the goal of helping local manufacturers compete within the global market. An example of this being the SANS 1804-1,2,3&4 standards that are based on the IEC 60034 series of publications. It should thus be safe to assume that as Europe updates its MEPS based on new publications from the IEC or CENELEC, the SABS will eventually also update its standards accordingly.

The European legislation that set the MEPS for electric motors in 2009 was based on the IEC 60034-30 standard which was first published in 2008. This standard introduced the IE classifications as a means to facilitate fair competition and market development globally. Since then the standard has been revised and split into two versions, namely the IEC 60034-30-1 standard which deals with most LV motors intended for direct-on-line operation, and the IEC TS 60034-30-2 technical specification (TS) which applies to most LV AC motors rated for variable speed operation. These publications define the IE-classes and their efficiency limits according to supply frequency, number of poles and rated power and provide interpolation equations for motors with rated power not listed in the tables [9].

In order to assign an IE-class to any motor that falls within the scope of either IEC 60034-30-1 or IEC TS 60034-30-2, the motor must be tested according to the respective general requirements and methodologies as set forth in IEC 60034-2-1 and IEC TS 60034-2-3. It is important to note at this point that while the scope of IEC TS 60034-2-3 is currently limited to the

efficiency determination and separation of losses of VSD operated IMs, the input-output method (2-3-C) already applies to other motor technologies and may be used to determine their IE-class. Also, it is expected that the next revision of IEC TS 60034-2-3 will be expanded to include testing procedures for VSD operated synchronous motors [10].

So far the regulations and standards they are based on have only dealt with the efficiency determination and classification of electric motors. There is however a growing trend in industry of using VSD operated motors where possible. With foresight on this, CENELEC published EN 50598-1&2 standards in 2014 as requested by mandate under the European Ecodesign Directive [1]. These standards have since been used as the basis for the newly published (2017) IEC 61800-9-1&2 standards. The standards hold that the needs of the application should be considered along with different motor systems in order to best gauge the most energy efficient solution.

The standards define a frequency converter with all its control circuitry as a Complete Drive Module (CDM). The combination of a CDM or motor starter with an electric motor of any type within the scope of the standard is defined as a Power Drive System (PDS). The extended product is then the combination of a PDS with its intended driven equipment [11]; see Fig. 2.1 for a graphical representation of the extended product limits.

Part 1 of the standard defines the Extended Product Approach (EPA) methodology, and requirements for the Semi-Analytical Models (SAMs) that

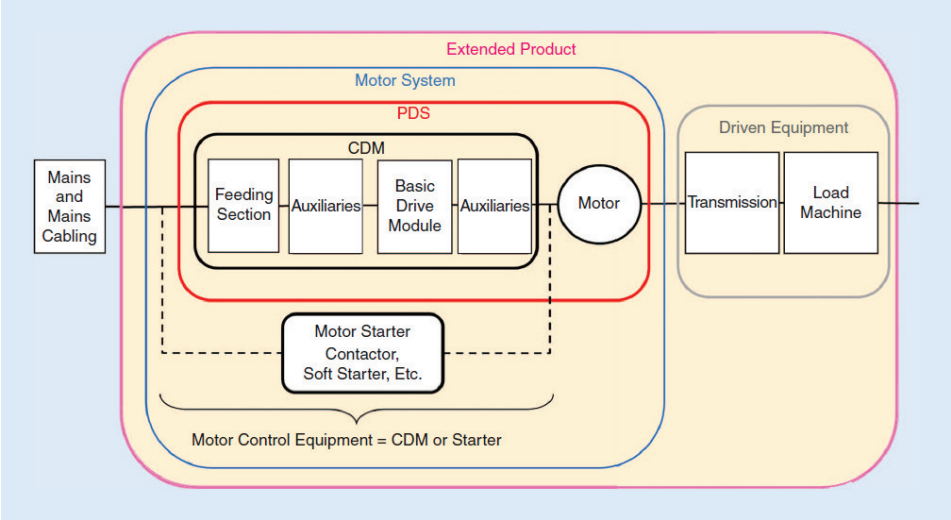

Figure 2.1: Extended Product Definitions (Source: [1])

are always required in the electrical system analysis of any extended product and its sub-parts [11]. It is also intended to serve as a reference base for regulators and minimum energy performance standards.

Part 2 defines new IE-classes for CDMs and IES-classes for PDSs, together with their limit values, and the test procedures by which the classifications are assigned. As part of this, the standard gives the losses of a reference motor (RM), reference PDS (RPDS) and reference CDM (RCDM) and the mathematical model for their calculation. The measured losses of the real PDS or CDM are compared against the reference values to determine the IE/IES-class [11]. The RM and RCDM can also be used to determine the efficiency class of a motor system when one of its constituents is unknown.

2.2 Reluctance Synchronous Machines

Synchronous reluctance machines have been around since before the 1960's in various forms, but didn't find widespread adoption due to relatively high torque ripple and low power factor when operated in open loop fashion, resulting in machines that were noisy and not especially efficient.

In the last three decades the world has seen rapidly improving microprocessor and switch technology, which has led various researchers to consider the possibility of whether the RSM may benefit from these advances.

It was found that carefully controlling the stator currents could improve the torque density and efficiency of the machines, making the performance of the RSMs comparable, and perhaps even superior, to IMs [3; 12]. This was shown analytically in [12] using lumped parameter models of the RSM and IM, with conservative values assigned to key parameters.

A design based comparison of IM, RSM and PM motors in [13] shows how the RSM is capable of higher maximum torque than the IM, for same stack volume and copper losses. This result is also reflected experimentally in [14]. At the same time the authors show how the optimal torque and power factor of the machines are found at different air-gap diameters, which is important to consider when comparing RSMs and IM with the same stator stack.

2.2.1 Design Aspects

Analysis done in [15] provides a theoretical approach to calculating the number of flux-barriers required, in relation to the number of stator slots, to provide for the smallest possible torque-ripple. This approach is verified experimentally and the results make it clear that with a combination of the right number of properly positioned flux-barriers, stator-chording, and skewing of the rotor, the torque-ripple problem can be all but eliminated. Fig. 2.2(a) shows the result for a RSM with 36 stator slots. The effects of stator chording and rotor skewing are also investigated in [16] using a combination of theoretical and FEM analysis.

As available computing power has increased and advancements have been made in optimisation methods and software, researchers have begun to focus a lot more on the design of the rotor. Ever more complex flux-barrier shapes are being experimented with and fine tuned using the optimisation software in an effort to obtain the best possible results for torque density, torque ripple, and power factor.

In [4] the authors employ a complex flux-barrier shape which is based on the principles of fluid dynamics (see Fig. 2.2(b)). The chosen shape is very simple to generate, requiring as little as two free variables per barrier during optimisation [5], while also making good use of the available rotor area. This allowed for an extensive comparison to be made of the torque, torque-ripple, and iron losses of optimised 4-pole RSMs with stator slots numbering 12, 24 and 48, and flux-barriers numbering 1 to 6 per pole. The results indicate that high numbers of stator slots and flux-barriers are preferable for attaining good

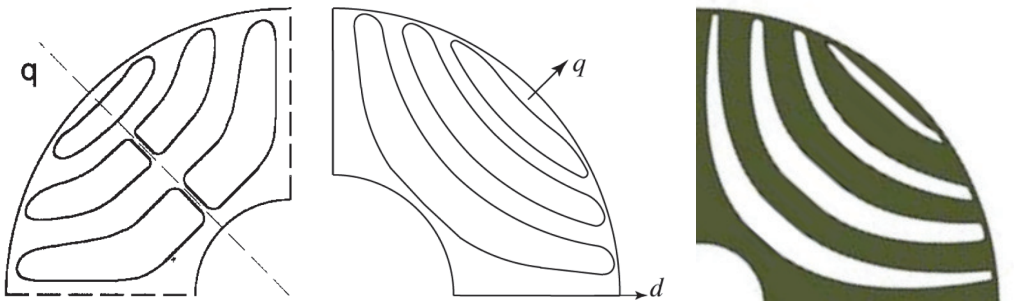

(a) Optimised I2U [15] (b) Fluid-barrier design [5] (c) Asymmetrical design [6]

Figure 2.2: RSM flux-barrier designs.

torque and power factor, and that minimisation of torque-ripple and iron losses require precise matching of number-of-flux-barriers to number-of-stator-slots. The authors go further by showing how their results for best torque-ripple confirm the results of [15].

In [6] the authors investigate the feasibility of using fully asymmetrical flux barrier shapes (see Fig. 2.2(c)) as a means to achieve low torque-ripple. It was found that with this type of design, torque ripple below 5% is achievable without compromising the maximum torque capability of the RSM. At the same time an extensive study was made of the effects of the current angle and rotor skewing on the torque ripple of the asymmetrical designs. The results show that the ripple can be further reduced significantly by skewing the rotor by a fraction of the stator slot pitch, and that the current angle also clearly influences the torque-ripple.

2.2.2 Encoderless Control

The need for precise knowledge about the rotor position of the RSM to achieve usable performance has always been one of its drawbacks. Shaft transducers are commonly used to determine the rotor position, but these come with problems of their own and they also increase the price of the system substantially. Fortunately the RSM's inherent saliency lends itself well to the application of sensorless control.

There used to exist only two primary approaches to sensorless control. The first of these are the fundamental excitation methods, as in [17], that track the fundamental saliency of the machine. These methods work very well at medium to high speeds, but fail at lower speeds and standstill due to the lack of back EMF. The second approach is dependent on high frequency [18], or pulsed[19], voltage injection that allows the rotor position to be determined from the machine's response. These methods are excellent for standstill to medium speed operation, but they fail at high speeds due to the back EMF impairing the voltage supply's ability to inject the required signal. Combinations of these methods have also been attempted, but the crossover point between the schemes creates new problems.

In [17] the authors address the issue of control instability due to saliency shift by proposing a control scheme that takes into account the non-linear behaviour of the flux-linkages under saturation and cross saturation. A linear

scheme is derived analytically and extending to include the non-linear effects of the machine. Except for a slight oscillating tracking error at high currents, that the authors attribute to a superimposed stator saturation effect, the experimental validation of the scheme shows it to be very capable for medium to high speeds.

A slightly different inductance saliency based approach is proposed in [20] that exploits the voltage states which occur due to time shifts in the PWM signal to extract saliency position information from the stator currents. This approach is built on the principles of predictive torque control and since it doesn't require any additional signal injection it is capable of operating at all operating speeds, making it the first encoderless scheme that could do this.

2.2.3 Applications

The earliest application that the RSM was used for was in fibre spinning plants where the ability of the RSM to run at synchronous speed allowed for a higher quality synthetic fibre to be produced [12]. However, due to its inherent problems the RSM had at the time, adoption rates were very low. Fast forward to today and it is clear that the RSM still hasn't found widespread adoption, although it appears as though this is starting to change.

With the advances in power electronics and encoderless control methods, which allow the RSM to be used to it's full potential, the technology is now considered mature enough for RSM drive packages to be offered by large companies, like ABB [21] and SIEMENS AG [22], for various applications. Also, because the RSM is always driven by a frequency converter, the inherently low power factor of the machine only affects the inverter rating and isn't apparent on the grid supply. Taking these facts into account, along with the expansion of global efficiency regulations and standards, it becomes clear why industries are starting to take notice of the RSM's advantages.

Much of the research that has been done into RSMs over the years state the intended application as pumps and fans, or squared-torque. This is due to the RSM not suffering the same performance degradation at partial loads as the IM, giving it the ability to maintain relatively high efficiency levels and making it a prime candidate for these types of applications.

While not as often considered, electric vehicle applications that require field weakening operation has also been the topic of research regarding the RSM

over the last ten years. Even though RSMs don't posses the extended field weakening region required by electric vehicles for direct-drive approaches [23], it has enough to be considered a viable choice for geared solutions [24]. The relatively small size and high efficiency of the RSM also make it an attractive candidate in this field.

When it comes to constant torque applications the RSM also performs very well due to the direct relation between the applied current vector and the torque it produces. Interestingly however, the RSM's overload capability at low speeds also make it ideal for extruders where high starting torque is required to set the process in motion. In the past only DC motors were able to fill this role, but the RSM has proven itself capable. As an added advantage, the RSM doesn't have any brushes that need regular maintenance, which significantly reduces operational costs and downtime.

Chapter 3

RSM Design and Performance

The research question is answered through a combination of finite element method (FEM) simulations, theoretical analyses, optimisation, validation, and experimentation. The methods by which this design is implemented are described in this chapter, while the optimisation and validation of the RSM is covered in Chapter 4.

3.1 Induction Machine

A general purpose motor with an IE3 efficiency rating, manufactured by WEG, has been chosen for the comparison. According to the regulations it would have been permissible to use an IE2 motor, but it was decided that an IE3 IM would be more relevant. Furthermore, the chosen IM is built using copper wire with class H (180 °C) thermal insulation which has greater resilience against the damage caused by the voltage spikes that are common to inverter operation.

To make the comparison as fair as possible, two of the IMs have been acquired and one was opened and stripped of all parts. An internal view of the chosen IM is visible in Fig. 3.1 and the most pertinent information from the IM's nameplate is summarised in Table. 3.1. The IM's frame, shaft, bearings and fan are reused in constructing the RSM in order to exclude their influence in the comparison. The RSM is also designed with the same stack length as the IM to exclude any effect that having differing stack volumes may have, and to allow for conclusions to be drawn about the RSM's efficiency potential based on having the same stack volume as the IM. As a final measure to keep

Figure 3.1: Induction machine internal view.

Table 3.1: Induction machine nameplate values

Frame	V	Hz	kW	RPM	A	PF	IE Code	100%	75%	50%
132S	380	50	5.5	1460	10.7	0.87	IE3	89.6%	89.6%	89.0%

the comparison fair, the RSM is also designed with the same number of stator slots as the IM.

3.2 Designing the RSM

This section deals with the decisions that were made regarding the design of the RSM, as well as the implementation of those decisions in the FEM model.

3.2.1 Stator Topology

In many studies involving the RSM, for example [14] and [23], the authors decide to retrofit an induction motor by replacing the rotor, and perhaps the windings, while keeping the stator intact. This is possible because the design

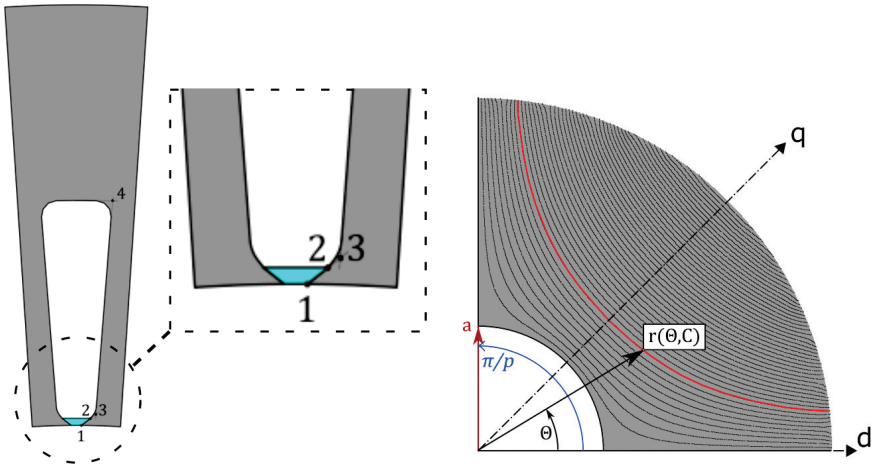

(a) Stator slot shape. (b) Flux lines in solid rotor

Figure 3.2: Stator Slot and rotor flux-barrier designs.

considerations for the stators and windings of IMs and RSMs are very similar. The problem that arises from this is that using IM's stator may not allow for the optimal sizing of the RSM's rotor, with the implication being that the RSM might perform better if a stator is specifically designed for it [13]. Based on this the decision was made to include the stator in the design optimisation.

A highly variable, although symmetrical, slot shape has been chosen for the stator design with the intent of increasing the number of potential slot designs that can be investigated. As shown in Fig. 3.2(a), four points determine the overall shape of the slot. Points 1 to 4 are connected using straight lines, and point 4 is connected to the symmetry axis by a circle segment that is concentric to the outside of the stator. Fillets of any reasonable radius can be placed at points three and four, and the slot area can be split in half, horizontally, to allow for double layered windings. Limits are set within the design code to ensure that only slot shapes that are within manufacturing tolerances can be generated.

Except for the inner and outer stator diameters, the variables that determine the shape of the stator can either be defined to all be relative values, to facilitate optimisation, or real values, for recreation of specific stators. As an added feature the design code is also able to determine the maximum and minimum inner diameter of the stator, based on given limits, to further simplify its implementation in the optimisation.

3.2.2 Rotor Topology

Determining the best flux barrier shape is outside the scope of this study and so a design strategy, based on the work done in [4], has been chosen. Therein the basic flux barrier shape is based on the principles of fluid dynamics. The design is achieved by using field lines that describe the flow paths of a fluid channelled by two infinite plates, stretching out from the origin and forming an angle π/p between them, with a plug of radius a centred at the origin (see Fig. 3.2(b)). In terms of an electric motor, the field lines may be interpreted as magnetic flux lines in a solid rotor with a non-magnetic shaft [4].

The two equations that are used to define the basic shapes of the flux barriers are given in [4] as:

$$C(r,\theta) = \sin(p\theta)\frac{(\frac{r}{a})^{2p} - 1}{(\frac{r}{a})^{p}} \tag{3.1}$$

and

$$r(C,\theta) = a\sqrt[p]{\frac{C + \sqrt{C^2 + 4\sin^2(p\theta)}}{2\sin(p\theta)}} \qquad \text{for} \qquad 0 \leq \theta \leq \pi/p \tag{3.2}$$

Here, r and θ are the radius and angle, in polar coördinates, of any point in the plane, C is a constant that determines which field line has been chosen, a is the radius of the shaft and p is the number of pole pairs.

The flux barriers lines are generated according to the following procedure:

1. Calculate the distance (r) from the origin where the barrier line crosses the symmetry axis, or q-axis, of the rotor.
2. Calculate C for this radius by using (3.1), with θ set to $\pi/(2p)$.
3. Substitute the rotor outer radius and C into (3.1) and solve for θ to find the angle where the barrier line meets the rotor circumference.
4. Substitute C into (3.2) and vary θ within the limits calculated in step 3 to generate the nodes of the flux barrier line in polar coördinates.

The ribs are formed by fitting circular fillets tangential to both the flux barrier lines and the circles, centred at the origin, that determine the heights of the ribs.

As with the stator, limits are set within the design code to ensure that the generated rotors are within manufacturing tolerances. Also, the variables that

determine the positions and heights of the flux barriers, can either be defined to all be relative values, to facilitate optimisation, or real values, for recreation of specific rotors. The design code is also able to determine the maximum and minimum outer diameter of the rotor based on the shaft diameter and given limits.

3.2.3 Constant Design Parameters

Table. 3.2 gives the list of design parameters that are chosen as constants for the purpose of this study. As discussed in section 3.1, the values given to the *Stator Diameter*, *Stack Length*, *Number of Stator Slots*, and *Shaft Diameter* have all been chosen to match the IM.

The width of the stator slot at the air gap has been chosen to allow for a reasonably sized magnet wire to be wound into the slots. The air gap height represents common practice for 5.5 kW, 4 pole IMs as found in literature. The height of the ribs are chosen based on manufacturing constraints. The number of flux barriers per pole for a 48 slot RSM is used as calculated in [4], with the goal of allowing for the smallest possible torque ripple. Also, two winding layers are used to allow for a coil span of 10/12, which is the standard chording used to minimise the magnitude of the 5^{th} and 7^{th} harmonic flux waves [16] and their contribution to the torque ripple. The copper fill factor value of 0.45 is considered reasonably conservative when designing for stranded coils. Finally, the use of four parallel winding circuits is to allow for finer voltage resolution when the number of turns per coil is calculated.

Table 3.2: Design Parameters

Parameter	Value
Stack Length	131 mm
Stator Diameter	220.5 mm
Number of Stator Slots	48
Shaft Diameter	48 mm
Stator Slot Opening	1.0 mm
Air Gap	0.34 mm
Rib Heights	0.5 mm
Number of Flux Barriers per Pole	4
Number of Winding Layers	2
Coil Span	10/12
Copper Fill Factor	0.45
Parallel Winding Circuits	4

Table 3.3: Design Variables

Parameter
Rotor Outer Diameter
Total Height of Flux Guides
Heights of Flux Guides
Heights of Flux Barriers
Stator Slot Angles and Radii
Turns per Coil Side
Current Density and Angle

3.2.4 Variable Design Parameters

The parameters given in Table. 3.3 represent all the degrees of freedom in the design model for the RSM. The variables controlling the rotor topology (flux guides, -barriers and rotor diameter) together with the variables that determine the shape of the stator slots (see Fig. 3.2(a)) are the most important as these parameters are primarily responsible for the overall performance of the machine. As such they are allowed to vary as much as possible, within the limits of the material, in order for the widest range of topologies to be simulated.

The inclusion of the *Turns per Coil Side* parameter, which refers to the number of conductors per winding layer in each stator slot, allows for the RSM's rated voltage and current to be adjusted and, once the power factor is determined, for the inverter losses to be calculated. Current density and angle are also included as variable parameters to allow for the best operating points to be identified. These parameters are kept within reasonable limits to avoid unnecessary simulations.

3.3 Calculating Performance

This section deals with the methodology and mathematical model that are used to determine the performance of the simulated RSM and VSD.

3.3.1 FEM Analysis

When designing the RSM, a combination of FEM and theoretical analysis is used to estimate the performance of the motor. The electromagnetic analysis of the RSM is done by use of a non-commercial FEM program called SEM-

FEM, which is an in-house developed FE simulation package that uses static simulations to generate solutions. This program has the advantages of being flexible and easy to use, employing python scripting to operate, as well as having reduced solving time when compared to commercial FE packages.

Solution arrays are obtained from SEMFEM through multiple simulations with the rotor angle displaced from 0 to 120 electrical degrees. The torque array output is used to calculate average torque (T_{avg}), which is used to find the developed power (P_{dev}), and torque ripple (T_{rip}), which is calculated according to

$$T_{rip} = 100\% \times (T_{max} - T_{min})/T_{avg} \tag{3.3}$$

SEMFEM also provides arrays containing the per-phase flux-linkages, and graphs containing data on the flux-density in each mesh element. The flux-linkages are transformed into their dq-components (λ_d and λ_q) to calculate voltages during post-processing (Eq.3.4), and the flux-density graphs are used to estimate the core losses (P_{core}) in the motor (see section 3.3.3).

3.3.2 Reluctance Synchronous Machine

The theoretical part of the analysis is based on the steady-state dq equivalent circuits and space phasor diagram shown in Fig. 3.3. The simulation results from SEMFEM and the following equations are used to estimate the performance of the RSM.

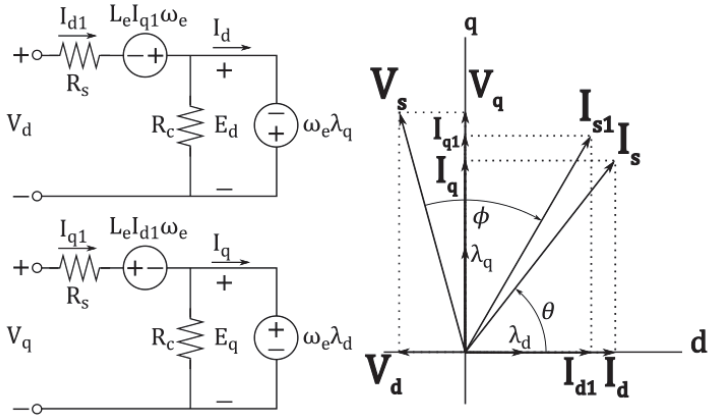

Figure 3.3: DQ equivalent circuits and space phasor diagram of RSM.

The speed voltages E_d and E_q are calculated using [25]:

$$E_d = -\omega_e \lambda_q \qquad E_q = +\omega_e \lambda_d, \tag{3.4}$$

where ω_e is the electrical speed of the rotor reference frame and λ_d and λ_q are the d- and q-axis flux-linkages, making the rms induced voltage

$$E_a = \sqrt{0.5(E_d^2 + E_q^2)}. \tag{3.5}$$

Once the core losses (P_{core}) have been calculated (see Section 3.3.3), the core resistance R_c is then derived using

$$R_c = 3E_a^2/P_{core}. \tag{3.6}$$

With R_c now known, the d- and q-axis supply currents are calculated as

$$I_{d1} = I_d + E_d/R_c \qquad I_{q1} = I_q + E_q/R_c, \tag{3.7}$$

making the rms phase current

$$I_{s1} = \sqrt{0.5(I_{d1}^2 + I_{q1}^2)}. \tag{3.8}$$

The steady-state d- and q-axis supply voltages V_d and V_q are then calculated using

$$\begin{aligned} V_d &= E_d - L_e I_{q1} \omega_e + I_{d1} R_s \\ V_q &= E_q + L_e I_{d1} \omega_e + I_{q1} R_s, \end{aligned} \tag{3.9}$$

where the end-winding leakage inductance (L_e) and the stator copper resistance (R_s) are approximated analytically according to methods discussed in Section 3.3.4 and Section 3.3.5 respectively. Now, with the supply phase voltage calculated as

$$V_{s1} = \sqrt{0.5(V_d^2 + V_q^2)}, \tag{3.10}$$

and the power factor of the RSM determined according to

$$\begin{aligned} \phi &= \text{atan}(V_q/V_d) - \text{atan}(I_{q1}/I_{d1}) \\ Pf &= \cos\phi, \end{aligned} \tag{3.11}$$

the input power (P_{in}) supplied to the motor, and the output power at the shaft (P_{out}) are calculated using

$$P_{in} = 3V_{s1}I_{s1}\cos\phi; \qquad P_{out} = \omega_m T_{avg} - P_{add}, \tag{3.12}$$

with T_{avg} the average torque, ω_m the mechanical speed of the rotor, and P_{add} representing the additional load losses (see section 3.3.6). The final step is then to find the efficiency of the drive system (η_{DS}) and its components with

$$\begin{aligned} \eta_{MUT} &= (P_{out}/P_{in}) \times 100\% \\ \eta_{inv} &= (P_{in}/(P_{in} + P_{inv})) \times 100\% \\ \eta_{DS} &= \eta_{MUT} \times \eta_{inv}, \end{aligned} \tag{3.13}$$

where the inverter losses (P_{inv}) are calculated according to the method given in section 3.3.7.

3.3.3 Core Losses from Steinmetz

Core losses are very difficult to model with any real accuracy. There are many possible sources with varying influence that can't be easily accounted for. Adding to the problem is the difficulty of finding complete and accurate loss tables. As such, a modified version of Steinmetz's core loss equation is used and is applied for only the fundamental supply frequency (f_1) as

$$P_{core} = c f_1^x (B_{tooth}^y M_{tooth} + B_{yoke}^y M_{yoke}) k_{exp}. \tag{3.14}$$

In (3.14), B_{tooth} and B_{yoke} are the maximum flux densities in the stator teeth and yoke taken from the simulation results. The iron masses of the teeth and yoke (M_{tooth} and M_{yoke}) are calculated from their respective cross sectional areas and the active stack length. The Steinmetz coëfficients (c, x & y) are determined by fitting a curve to the M400-50A loss tables at frequency f_1. The k_{exp} term in (3.14) is an experience factor based on industry practice. Its purpose is to account for the underestimation of iron losses in rotating machines by analytical models and FEM packages. For the purpose of this study it is assumed that this factor also accounts for the additional harmonic losses due to converter operation when given the value of 1.8.

3.3.4 End-Winding Leakage Inductance

For the purpose of this study, the per-phase end-winding leakage inductance is calculated according to the formula given in [25] for elliptical-shaped winding ends as

$$L_e = V_2 m d_i \left[\frac{W k_d k_{p(2)}}{p}\right]^2 k_{e(2)} \times 10^{-8} \text{ H}, \tag{3.15}$$

where

V_2 = Shape factor for elliptical double-layer winding ends
m = Number of phases
d_i = Stator inner diameter [meters]
W = Number of turns in series per phase
k_d = Winding distribution factor
$k_{p(2)}$ = End-winding coil pitch factor for elliptical coil shapes
p = Number of pole pairs
$k_{e(2)}$ = 2 pole pair end-winding factor

with $V_2 = 920$ and $k_{e(2)} = 0.595$. The winding distribution factor is found by using [25] as

$$k_d = \frac{\sin(\pi/6)}{q\sin[\pi/(6q)]}, \tag{3.16}$$

while the formula for the end-winding coil pitch factor for elliptical coil shapes is given as

$$k_{p(2)} = \frac{3\sin[(\pi c)/(6q)]}{4 - [c/(3q)]^2} + \sin\left(\frac{\pi c}{6q}\right), \tag{3.17}$$

where q is the number of stator slots per-pole per-phase and c is the coil pitch in terms of number of stator slots.

3.3.5 Stator Copper Resistance

Continuing to follow the methodology of [25], the stator winding copper resistance is calculated according to the given formula

$$R_s = 2W\rho_t\left(\frac{l + l_e}{n_a A_{\mathrm{Cu}}/z}\right)\ \Omega, \tag{3.18}$$

where

W = Number of turns in series per phase
ρ_t = Resistivity of copper at temperature t_c
l = Stack length of the motor
l_e = Average length of a winding end
n_a = Number of parallel winding circuits
A_{Cu} = Active copper area per stator slot
z = Number of conductors per stator slot.

The resistivity coefficient (ρ_t) is found using

$$\rho_t = \rho_{20}[1 + Y_t(t_c - 20)], \tag{3.19}$$

with $\rho_{20} = 17 \times 10^{-9}$ Ω.m, $Y_t = 0.0039/^{\text{o}}\text{C}$, and for a winding temperature of $t_c = 75^{\text{o}}\text{C}$.

3.3.6 Additional (Stray) Load Losses

When an electric motor is operating under load, there is another loss component not accounted for by the standard models and equations. This is known as stray- or additional load losses. These losses are non-negligible and are very difficult to model with any accuracy without expending great effort to model the entire machine with 3D FEM and applying a detailed analysis of core losses.

The author has been unable to find any study that has been done on the stray load losses of the RSM, and so has opted for using the assigned allowance for additional load losses in induction machines from IEC 60034-2-1 (8.2.2.5.3). It is however expected that, due to the lack of conductors on the rotor, the stray load losses for the RSM should be significantly lower than for the IM.

For the purpose of this study, additional load losses are based on the developed power $P_{dev} = \omega_m T_{avg} \times 10^{-3}$ and are calculated using [26]

$$P_{add} = \begin{cases} 0.025 P_{dev} & \text{if} \quad P_{dev} \leq 1 \text{ kW} \\ \left[0.025 - 0.005 \log_{10}\left(\dfrac{P_{dev}}{1 \text{ kW}}\right)\right] P_{dev} & \text{if } 1 \text{ kW} < P_{dev} < 10 \text{ MW} \\ 0.005 P_{dev} & \text{if} \quad P_{dev} \geq 10 \text{ MW} \end{cases} \tag{3.20}$$

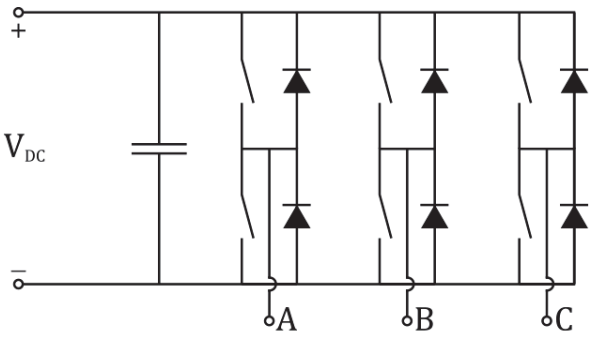

Figure 3.4: Three-phase, two-level, voltage source inverter.

3.3.7 Inverter Losses

A two-level voltage source inverter as shown in Fig. 3.4, employing sinusoidal PWM with no over-modulation, is chosen according to the specifications given in [27]. Therein it is specified that when determining the efficiency of an inverter driven motor with a power rating of up to 90 kW, a switching frequency of 4 kHz must be used.

Equations (3.21) to (3.23) are the equations for the power losses in the IGBTs and diodes of the two-level voltage source inverter employing sinusoidal PWM [28]. The IGBT switching losses are calculated by

$$P_{switch} = \frac{f_s}{2\pi} V_{DC} I_0 (t_{on} + t_{off}), \tag{3.21}$$

where f_s is the switching frequency of the inverter, V_{DC} is the DC-link voltage, $I_0 = \sqrt{2} I_{s1}$ (with I_{s1} from Eq. 3.8) is the peak value of the line current of the motor, and t_{on} and t_{off} are the on/off switching times of the IGBTs. The IGBT conduction losses are determined by

$$P_{cond} = V_{on} I_0 \Big(\frac{1}{2\pi} + \frac{m_a \cos\phi}{8} \Big), \tag{3.22}$$

where V_{on} is the IGBT's on-voltage when conducting, m_a is the modulation index, and $\cos\phi$ is the power factor from (3.11). The diode losses are calculated by

$$P_{diode} = V_{diode} I_0 \Big(\frac{1}{2\pi} - \frac{m_a \cos\phi}{8} \Big), \tag{3.23}$$

with V_{diode} the on-voltage of the diode. The total losses of the inverter are then calculated by

$$P_{inv} = 6(P_{switch} + P_{cond} + P_{diode}). \tag{3.24}$$

For the purpose of this study it is assumed that the rectifier losses has little effect on the outcome of the RSM's design optimisation. Hence, only the inverter losses are taken into account and the diode rectifier of the VSD is ignored.

3.4 Efficiency Classification (IE-code)

When this study began there wasn't any final decision from the IEC on how the IE-codes of motors intended for VSD operation would be determined and what the efficiency limits would be. However, in 2013 at the 8^{th} international conference on energy efficiency in motor driven systems (EEMODS'2013), Dr. M. Doppelbauer made a presentation on the proposed method by which the IE-codes of such motors could be determined, as cited in [9]. Dr. Doppelbauer is the convenor of the IEC technical committee (work group 31), which holds responsibility for the publication and maintenance of the IEC 60034-30-2 standard that deals with the IE-code classification of converter fed motors. As such it is the opinion of the author that Dr. Doppelbauer may be considered to be the relevant authority regarding this topic.

The proposal at the time was to determine the IE-code based on the measured efficiencies at seven operating points. Four of the operating points would account for constant torque applications, whereas the other three would gauge

Table 3.4: Proposed load points for constant torque applications.

Speed	Torque	Weighting Factor
100%	75%	0.20
75%	75%	0.30
50%	75%	0.30
25%	75%	0.20

Table 3.5: Proposed load points for square torque applications.

Speed	Torque	Weighting Factor
100%	100%	0.33
75%	50%	0.33
50%	25%	0.33

square torque performance. For these two application types the measured efficiencies would be weighted and summed, after which the average of the two values would be used to assign the IE-code. The proposed load points and their respective weighting factors are given in Table. 3.4 and Table. 3.5. The decision was made to use these operating points as the basis for the performance comparison between the RSM and the IM in this thesis.

It is important to take note that the standard concerned with efficiency classification of converter fed motors has now been published, as mentioned in Chapter 2. The testing requirements have been simplified to only require a single efficiency measurement at 100% torque and 90% speed, and the IE-class efficiency limits have been defined relative to the limits given in IEC 60034-30-1 through the use of Eq.3.25 [10].

$$\eta_n = \frac{1}{1 + (1 + r_{HL})(\frac{1}{\eta_{ref}} - 1)}, \tag{3.25}$$

where

η_n = New nominal efficiency limit

η_{ref} = Reference nominal efficiency limit from IEC 60034-30-1

r_{HL} = Efficiency de-rating factor = 15% for motors under 90 kW.

Applying Eq.3.25 to the IE limits for 4-pole, 50 Hz, 5.5 kW motors provides the new limits as 88.2% for IE3 and 90.8% for IE4.

Chapter 4

Optimisation

In this chapter the optimisation procedure is covered in more detail. Identifying the best optimisation algorithm is outside the scope of this thesis, so this section only gives an overview of the method used and the steps followed. More attention is paid to the definition of optimisation constraints and objectives. The chapter ends with the validation of both the simulated performance (Maxwell) and the objective (pyOpt).

4.1 Objectives & Constraints

Table 4.1 lists the simulation outputs that are, in turn, initially used as objectives and then subsequently used as constraints for the following iterations. These values are chosen based on the goals of the study, as well as to ensure that the RSM would be suitable for use in industry. The PDS efficiency objective is derived using the nameplate values of the IM and the inverter efficiency calculations from Section 3.3. The procedure by which these objectives and constraints are applied is explained in more detail in Section 4.2.

Table 4.1: Optimisation objectives & constraints

Parameter	Target
Rated Power	5.5 kW
Rated Voltage	380 V
Torque Ripple	$\leq$ 5.0 %
PDS Efficiency	$\geq$ 86.9 %

4.2 Methodology

Third party software called VisualDoc is used to control the optimisation. It allows for modular assembly of the optimisation procedure and has the ability to use external programs to run simulations and return to it any values required to track the objectives and constraints.

4.2.1 Algorithm (MMFD)

The Modified Method of Feasible Direction (MMFD) was chosen from available algorithms as it proved during initial testing to be robust in finding at least a local optimum within the feasible region. It is also relatively fast when compared to the other available methods. The algorithm is defined as follows:

Given the objective function $F(\mathbf{X}) : \mathbb{R}^K \rightarrow \mathbb{R}$, constraints $g_j(\mathbf{X})$, and lower and upper bounds on the design variables X_i^L and X_i^U, find a set of design variables $X_i; i = 1, ..., K$, contained in vector $\mathbf{X}$, that will

$$Minimise \ \ (\text{or Maximise}) \ \ F(\mathbf{X}) \tag{4.1}$$

subject to:

$$g_j(\mathbf{X}) \leq 0; \ \ j = 1, ..., M \tag{4.2}$$

$$X_i^L \leq X_i \leq X_i^U; \ \ i = 1, ..., K \tag{4.3}$$

The algorithm is given a starting vector $\mathbf{X}^0$ and then, beginning with iteration $q = 1$, the design is updated according to

$$\mathbf{X}^q = \mathbf{X}^{q-1} + \alpha^* \mathbf{S}^q, \tag{4.4}$$

where α^* is a scalar parameter that minimises $F(\mathbf{X})$ along the feasible search direction $\mathbf{S}^q$, and terminates when the convergence criteria are met.

Unfortunately there is no guarantee that the algorithm will find the global maxima, as is the case with gradient methods. Quantum methods, which have a much higher chance of finding the global maxima, are infeasible due to the large number of calculations required.

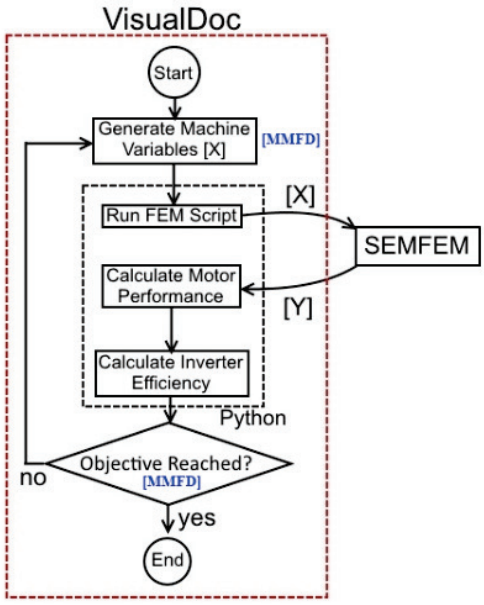

Figure 4.1: Optimisation procedure using VisualDoc (MMFD).

4.2.2 Procedure

The flow diagram in Fig. 4.1 depicts the procedure by which ViualDoc attempts to find an optimum using the design variables given in Table 3.3. The design optimisation is done in steps, optimising a single objective at a time while adding an additional constraint with each step, until an RSM topology is generated with the desired output characteristics. For the first and second step the current density is kept constant at 6.36 A/mm^2 and is allowed to vary for the third and forth steps. Thus, with the rotor speed (n) set equal to the rated speed (n_{rated}), the optimisation steps can be summed up as follows:

1. Maximise $F(\mathbf{X}) = P_{out}$, with the constraints $X_i^L \leq X_i \leq X_i^U; i = 1, ..., K$.
2. Minimise $F(\mathbf{X}) = T_{rip}$, adding the constraint $P_{out} \geq P_{rated}$.
3. Maximise $F(\mathbf{X}) = \eta_{RSM}$, with the additional constraint $T_{rip} \leq 5\%$.
4. Maximise $F(\mathbf{X}) = \eta_{DS}$, adding the final constraint $V_{LL} = \sqrt{3} \times Vdq = 380V$.

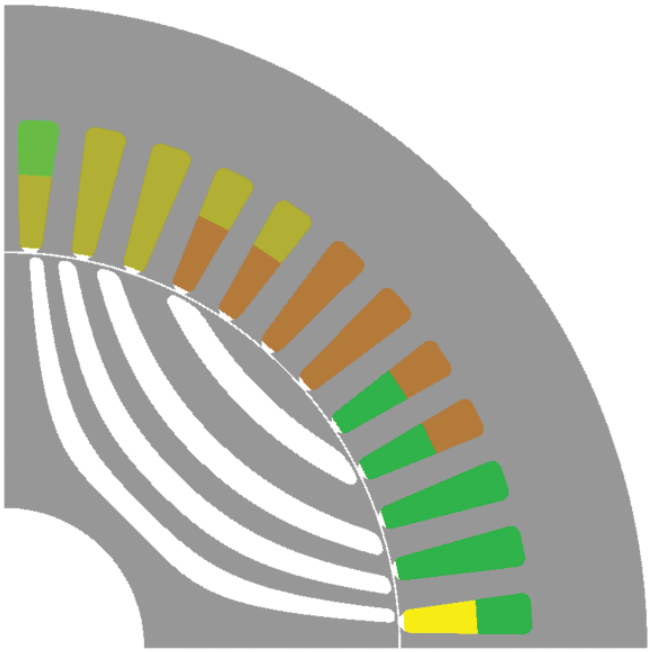

Figure 4.2: Cross section of RSM from SEMFEM.

4.3 Optimisation Results

4.3.1 Optimised RSM Design

Due to time constraints the VisualDoc optimisations were carried out as soon as it was believed that the model was generating reasonably accurate results. From these, the first viable result was chosen to be manufactured. A cross section of the optimised machine is shown in Fig. 4.2 with the corresponding machine parameters and expected performance given in Table. 4.2.

From the results in Table. 4.2, some conclusions may be drawn:

- The optimisation algorithm managed to find a design with drive system efficiency of 90 % which is significantly higher than the proposed objective of 86.9 % from Table. 4.1. This means that, from a simulation point of view, the research question has been answered to the affirmative. Furthermore, the result suggests that it should be possible to repeat the optimisation for a smaller frame size, perhaps with copper minimisation as the final objective, and still expect to find a feasible design.
- While it was expected that a high efficiency motor design would be

Table 4.2: Optimised RSM machine parameters and performance results

Parameter	Value
Rated Power	5.5 kW
Rated Torque	35 Nm
Power Factor	0.78
Rated Voltage	380 V
Rated Current	11.6 A
Current Density	3.64 A/mm^2
Current Angle	68.6^o
Copper Losses	170 W
Iron Losses	115 W
Assigned Stray Losses	117 W
Motor Efficiency	93.2%
Drive System Efficiency	90.0%
Torque Ripple	4.7%
Rotor Outer Diameter	135.3 mm
Aspect Ratio	0.614
Copper Weight	5.62 kg
Turns per Coil Side	34

generated, 93.2 % can still be considered to be very good. An efficiency result of this level means that the motor could at least be classified as an IE4 for VSD operation. If the IE5-class efficiency limits are set to reduce losses by an additional 20 % when compared to the IE4 limits, as has been suggested in [10], the RSM could even be rated as such.

- The power factor is relatively good. This implies that the power factor was indirectly optimised even though it wasn't used as one of the objectives or constraints. The likely reason is that its influence on inverter losses, and hence drive system efficiency, is significant enough to require its optimisation. What this means is that objectives that optimise the power factor more directly, like maximising torque per ampere, could generate similar results without specifically calculating inverter losses.
- The rated current is only 8.4 % higher than the IM's, which means that the RSM won't require a higher rated inverter. This would in turn lower the overall cost of the RSM drive system and so make the RSM a more attractive option in any installation where cost is a key deciding factor.
- At 3.64 A/mm^2 the current density is relatively low. If taken together with the copper weight of 5.63 kg, it indicates that the optimisation algorithm minimised the copper losses to improve the motor's efficiency, which makes sense as copper losses are dominant at this power level. However, this means that the copper isn't being used effectively, as totally

enclosed motors are generally designed for current densities nearer to 6 A/mm^2. The advantage this provides though is that the RSM should able to maintain high overload torque at low speeds for an extended period before temperature rise becomes a concern.

- The current angle of 68^o may be considered to be high, as RSMs are generally designed for a current angles in the low sixties or high fifties. One possibility for this result could be that a higher current angle was chosen as a way to improve the power factor and so reduce inverter losses, since the maximum power factor of a RSM is found at a higher current angle than its maximum torque.

4.3.2 Weighted Efficiency from Simulations

A procedure was created in Python that performs multiple simulations to find the seven desired operating points. It starts by simulating the RSM's performance on a relatively large grid of dq-currents which it then uses to estimate the point where the system efficiency is at a maximum for the desired output power. The procedure is then repeated with successively smaller grids around the estimates until the operating point is found. The resultant efficiencies together with their weighted values are given in Table. 4.3.

It is interesting to note that the system efficiency at rated conditions is slightly higher than for the operating point identified by the optimisation algorithm, even though the motor efficiency is lower. If the weighted motor efficiency was used to determine the IE-class, as was originally proposed in [9], the RSM would only have been eligible for an IE3 classification under the current efficiency limits. The weighted system efficiency is included in the table for the sake of interest.

Table 4.3: Variable speed & torque efficiencies

#	Torque	n [rpm]	Motor Eff.	System Eff.
1	35.0 Nm	1500	92.6%	90.3%
2	26.3 Nm	1500	92.5%	90.1%
3	26.3 Nm	1125	91.9%	88.8%
4	17.5 Nm	1125	91.7%	88.2%
5	26.3 Nm	750	90.5%	86.0%
6	8.8 Nm	750	89.6%	83.3%
7	26.3 Nm	375	86.1%	78.4%
Weighted:			90.9%	86.7%

4.4 Validation Studies

In the interest of due diligence, the optimised design is validated in two ways. The accuracy of the SEMFEM model is verified using ANSYS MAXWELL and the optimisation result is verified using a Python based optimisation algorithm SDPEN.

4.4.1 Maxwell

To verify that the SEMFEM model is generating accurate results, the RSM is recreated in Maxwell. As the post-processing analysis would be applied in the same way for the SEMFEM results as for the MAXWELL results, it is only necessary to compare the results of the static simulations of each program.

The torque is calculated for several current vectors and the results are compared against torque curves generated by SEMFEM for the same current magnitudes. Results of the comparison in the first and fourth quadrants are given in Fig. 4.3 and Fig. 4.4 respectively.

It was found that the output results agree reasonably well with the results given by SEMFEM. This implies that once the post-simulation analysis is

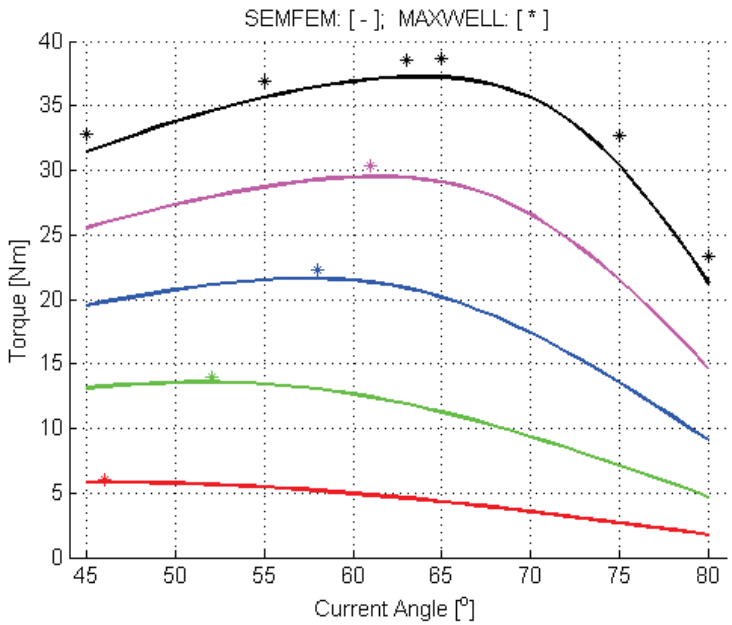

Figure 4.3: Validation of RSM motor torque using MAXWELL.

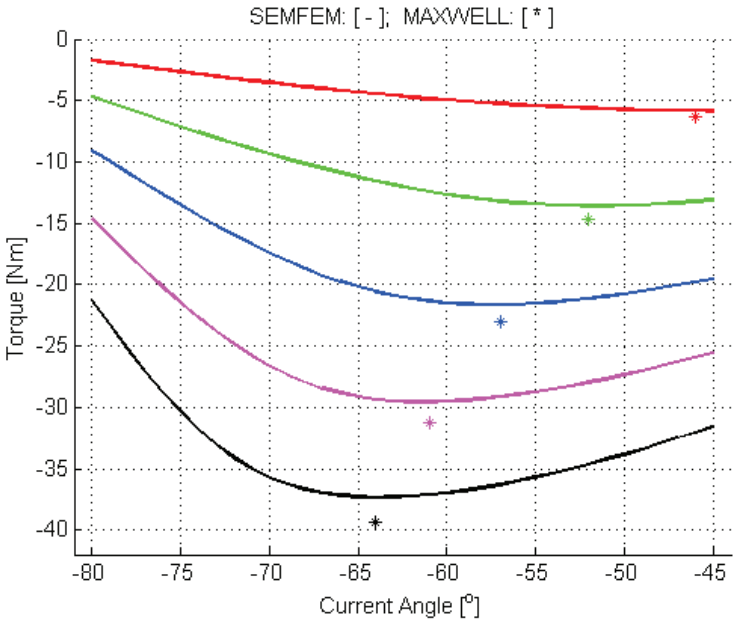

Figure 4.4: Validation of RSM generator torque using MAXWELL.

applied, the difference in final outputs will be within reasonable limits. This verifies the accuracy of the model created in SEMFEM.

4.4.2 PyOpt (SDPEN)

Verification of the optimised design is done using the pyOpt package for Python employing the *Sequential Penalty Derivative-free method for Non-linear constrained optimization* (SDPEN) algorithm.

While SDPEN allows for constraints to be programmed in, the decision was made to rather have it just optimise an objective function consisting of the sum of the weighted objective with quadratic penalty functions. The optimisation problem can be summed up as follows:

Given the objective function $F(\mathbf{X}) : \mathbb{R}^K \rightarrow \mathbb{R}$, constraints $g_j(\mathbf{X})$, and lower and upper bounds on the design variables X_i^L and X_i^U, find a set of design variables $X_i; i = 1, ..., K$, contained in vector $\mathbf{X}$, that will:

$$Maximise \quad F(\mathbf{X}) \tag{4.5}$$

subject to

$$X_i^L \leq X_i \leq X_i^U; \ i = 1, ..., K, \tag{4.6}$$

with

$$F(\mathbf{X}) = 100\frac{O(\mathbf{X})}{Target} - \sum P_j \left(g_j(\mathbf{X}) - C_j\right)^2, \tag{4.7}$$

where

$$\begin{aligned} O(\mathbf{X}) &= \text{Value of the parameter being optimised} \\ Target &= \text{Target value of the parameter being optimised} \\ P_j &= \text{Weight factor of penalty function } j \\ g_j(\mathbf{X}) &= \text{Value of constrained parameter } j \\ C_j &= \text{Limit of contraint } j \end{aligned}$$

The optimisation algorithm was allowed to run over the course of a month in which time it generated thirty feasible designs. The system efficiencies, motor efficiencies, and power factors are all plotted against copper mass in Fig. 4.5 to Fig. 4.7 respectively. While thirty designs isn't enough to generate true Pareto fronts, patterns do start to emerge from the data, and these are indicated by the red dotted lines.

What is interesting to see from Fig. 4.5 is that above 5.5 kg copper mass the system efficiency doesn't improve with the addition of more copper. When looking at Fig. 4.6 it is also apparent that the gain in motor efficiency is reduced significantly beyond this point. Furthermore, Fig. 4.7 shows a tendency for the power factor to decline as the copper mass increases, with the rate of declination increasing when the copper mass is above 5.5 kg. The behaviour of the PDS efficiency can be explained by the last two observations.

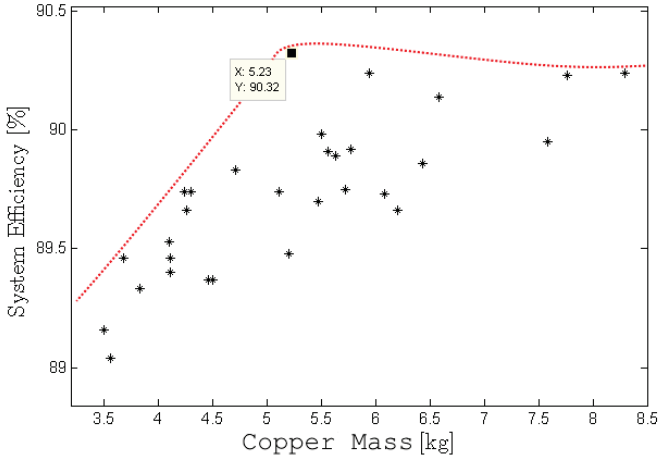

Figure 4.5: PDS efficiencies from SDPEN validation.

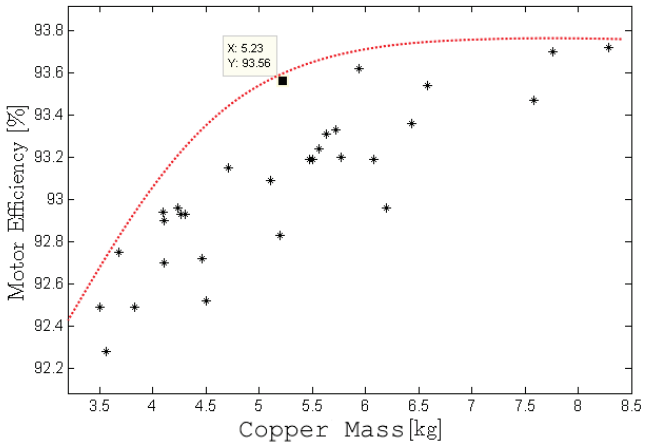

Figure 4.6: Motor efficiencies from SDPEN validation.

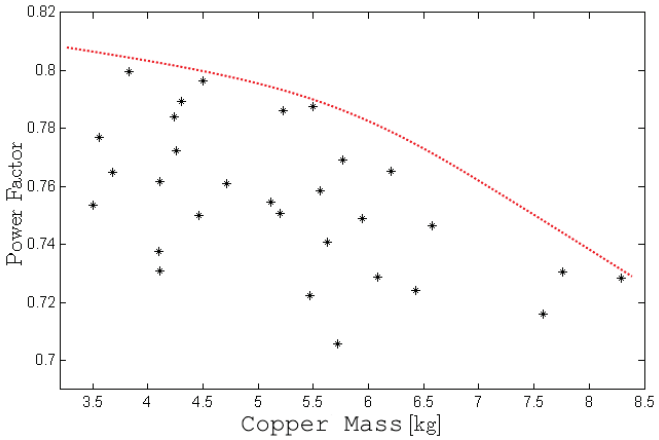

Figure 4.7: Power factors from SDPEN validation.

The data points given in Fig. 4.5 and Fig. 4.6 show the best result, with regards to copper utilisation, from the thirty optimised designs. For this design the system efficiency is practically the same as the design generated by VisualDoc, while the copper mass is 7.1 % less. It can thus be said that, even though there may still be some room for improvement in the VisualDoc design, the results agree enough to consider the design optimisation as valid.

Chapter 5

Experiments & Results

This chapter contains all the most pertinent results of the thesis. In sections 5.4 and 5.5 the results of the performance measurements for the RSM and the IM are given.

5.1 RSM Construction

The machine laminations were laser-cut from M400-50A electrical steel according to the optimised model of Section 4.3. The stator laminations and frame were assembled by the company hired to install the windings and is shown in

(a) Stator. (b) Rotor.

Figure 5.1: RSM stator and rotor assembly.

Table 5.1: Simulated RSM efficiencies (0.361 Copper fill factor)

#	Torque	n [rpm]	Motor Eff.	System Eff.
1	35.0 Nm	1500	91.8%	89.6%
2	26.3 Nm	1500	91.9%	89.5%
3	26.3 Nm	1125	91.0%	88.0%
4	17.5 Nm	1125	90.9%	87.5%
5	26.3 Nm	750	89.2%	84.9%
6	8.8 Nm	750	88.7%	82.3%
7	26.3 Nm	375	83.9%	76.6%
Weighted:			89.4%	85.3%

Fig. 5.1(a). The rotor was assembled in the university workshop and capped at the ends with stainless steel as shown in Fig. 5.1(b). The technical drawings for the rotor and stator are given in Appendix A.

Once the motor was assembled, it was discovered that the stator resistance was larger than analytically estimated. Investigation revealed that this was due to two factors: Firstly, due to a miscommunication between the author and the company responsible for winding the machine, it was wound with a thinner strand of magnet wire than was specified. This leading to the copper fill factor of 36.1% instead of the 45.0% used in the simulations. Secondly, the author underestimated the length of the end-windings.

The weighted efficiency of Table. 4.3 is recalculated with the stator resistance set to 0.66 Ω per phase, and the results are given in Table 5.1. The new simulated performance parameters of the RSM at rated conditions for a copper fill factor of 36.1% are given in Table 5.2.

Table 5.2: Recalculated RSM rated performance (0.361 Copper fill factor)

Parameter	Value
Rated Power	5.5 kW
Rated Torque	35 Nm
Power Factor	0.79
Rated Voltage	380 V
Rated Current	11.5 A
Current Density	4.55 A/mm^2
Current Angle	68.4^o
Copper Losses	257 W
Iron Losses	115 W
Assigned Stray Losses	117 W
Motor Efficiency	91.8%
Drive System Efficiency	89.6%
Torque Ripple	4.7%
Copper Weight	5.47 kg

5.2 Experiment Planning

The setup shown in Fig. 5.2 is designed with the intent of using the input-output method prescribed in [27] to determine the efficiency of both the IM and RSM systems. As the name implies, the method simply relies on measuring the power in and out of the motor to determine its efficiency. The method is extended to enable calculation of system efficiency as well.

The RSM and IM are connected shaft-to-shaft through a torque/speed sensor which enables one of the motors to be used as the load while the other is being tested. This also means that the machine that is loading the system is regenerating power back into the DC-link. The RSM is current controlled, using a control algorithm supplied by Mr. J. Mitchell (a master student at the time of the study), in order to control the system torque. The IM is controlled using the Volt-per-Hertz method and provides the speed control for the system. Torque sensor readings are saved on the laptop shown in Fig. 5.2.

Each motor is driven by a 22 kW SEW MOVIDRIVE frequency converter that receives its control signal from the FPGA installed in the pentium system, and sends back the phase A and B current measurements. As mentioned in Section 3.3.7, the frequency converters driving the motors are two-level voltage source inverters. The pentium control system employs space vector pulse width modulation (SVPWM), with no over-modulation, to generate the voltage waveforms at a switching frequency of 4 kHz. The IM's inverter is

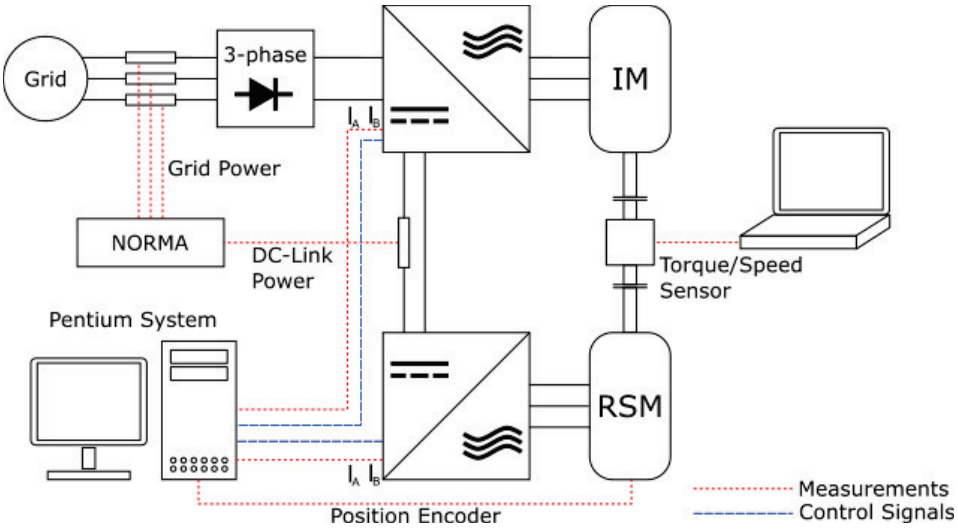

Figure 5.2: Test Bench Diagram.

powered from the grid and tied to the RSM's inverter through the DC-link bus. The diode rectifier shown in Fig. 5.2 exists internally within both the SEW converters, although the RSM drive diode bridge is omitted from the figure as its not in use.

The pentium system is designed in such a way to allow the user to program in any control scheme necessary while at the same time recording whatever available data are deemed important. It receives the phase current measurements from the converters through the Analogue-to-Digital Converters (ADCs), as well as the position encoder signal coming from the RSM, and returns the control signals to the inverters by way of the Digital-to-Analogue Converters (DACs). For the purpose of this study the Pentium system saves the measured dq-currents and reference voltage vectors for both machines together with the speed calculated from the position encoder.

A NORMA 5000 power analyser is used to measure the power flowing in from the grid, as well as the power flowing through the DC-link, and outputs the data to a laptop not shown in the figure. As the system is designed to be regenerative, the power reading from the grid is the total losses of the entire system, excluding the power consumed by the pentium system.

The one difficulty that arises with the setup is that there are three separate streams of data being collected simultaneously. Hence, before the data can be analysed, the collected data must be synchronised after the tests have been completed . This is accomplished by creating a pulse in the speed and reference current magnitudes at the start of data collection phase which, together with the data collected during the wind-down stage, can be used to align all three sets of data. The relevant data for each measured operating point are averaged over the last 25 seconds before the procedure steps to the next, which means that any error due to a small misalignment of the data is averaged out in the final analysis.

Once the data has been aligned and averaged, the resultant data points are used to calculate the performance of the systems. The motor efficiency of both machines are calculated the same way by using the fundamental component of the reference voltages and measured dq-currents recorded by the Pentium system to calculate the input power, and using the speed and torque measurements from the torque sensor to calculate the output power.

Due to the way the setup is planned, the system efficiency for each motor

needs to be calculated in a slightly different way. For the RSM the procedure is simplified by the fact that all the power flowing into its side is coming through the DC-link, and so the measurements from the NORMA and the torque sensor are enough to calculate the system efficiency. For the IM the situation is a little more complex, as for it the input power is coming both though the DC-link, as well as from the grid. Also, the losses in the 3-phase diode rectifier must be excluded in the interest of fairness as these losses aren't included for the RSM. Equation 5.1 is used to calculate the rectifier losses

$$P_{drect} = 2V_{on,drect}I_{in}, \tag{5.1}$$

with I_{in} being the grid phase-current measured by the NORMA, and $V_{on,drect}$ representing the voltage drop over the conducting rectifier diodes.

5.3 Test Bench

Figure 5.3 shows one of the initial test bench assemblies consisting of the motors, the dc-link tied inverters (Fig. 5.4), the Pentium system(Fig. 5.5), and the torque sensor which is hidden under the shaft safety cage. The resistor cabinet is there for protection purposes in the event the inverters need to dump

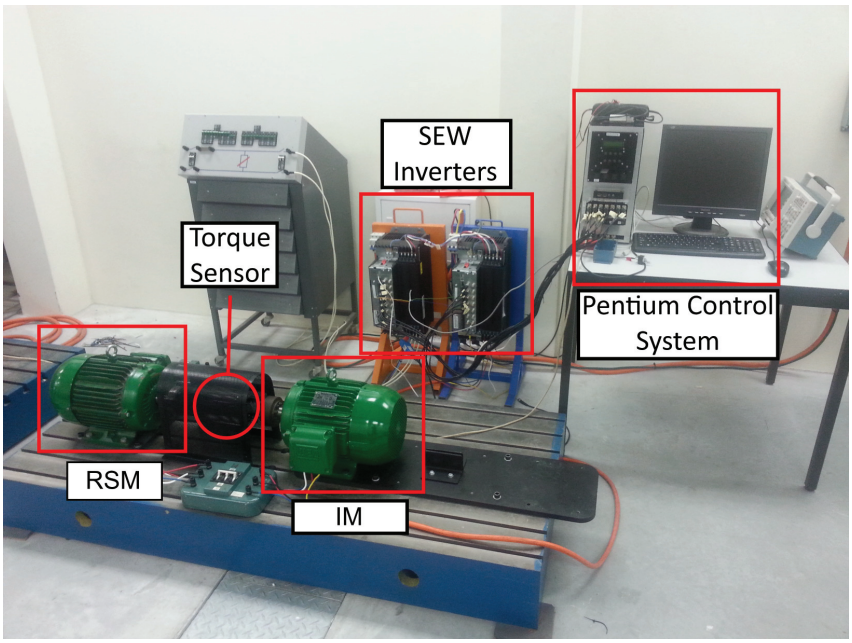

Figure 5.3: Preliminary setup of test bench.

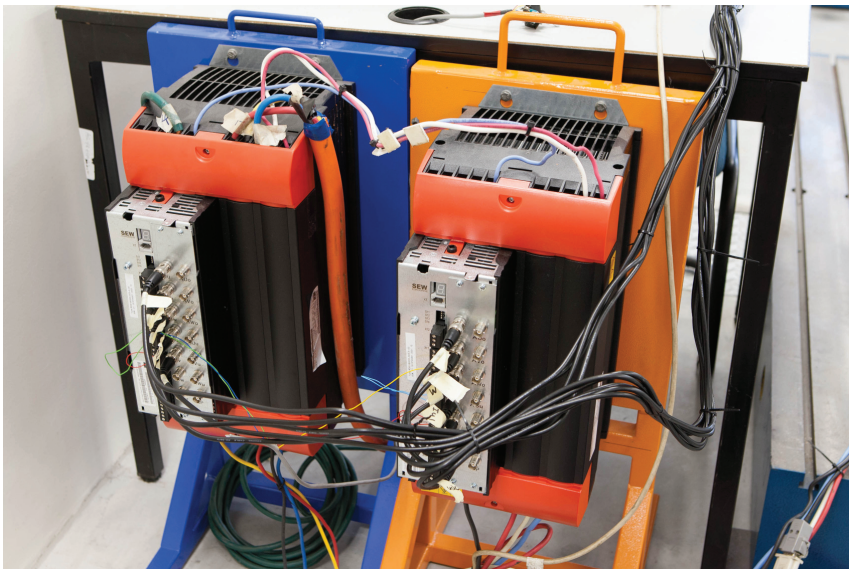

Figure 5.4: SEW 22 kW frequency converters.

energy through their breaking circuits. Each motor is connected through a 3-phase breaker which makes it possible for the phase resistances to be measured with minimum delay after the tests have been completed. In an effort to reduce electromagnetic emissions, screening was added to the cables leading to the resistor cabinet.

The test bench went through many trial assemblies before the finals tests

Figure 5.5: Pentium control system.

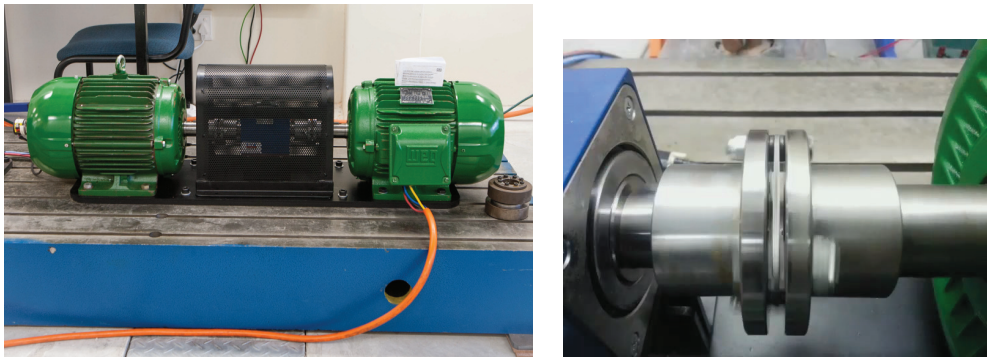

(a) RSM (left) and IM (right) (b) Flex coupling

Figure 5.6: Motors and flex coupling setup.

were run. A lot of effort was expended on aligning the shafts of the motors in the hope of eliminating as much vibrations as possible. This was done to assure the torque sensor's data quality, as well as to minimise any chances of damage to the sensor. A closer look of the RSM and IM is shown in Fig. 5.6(a), where both shafts were connected to the torque sensor through flexible couplings (Fig.5.6(b)). Visual inspection and measurements at low speed showed the presence of vibrations that the author deemed excessive, and so a different approach was taken.

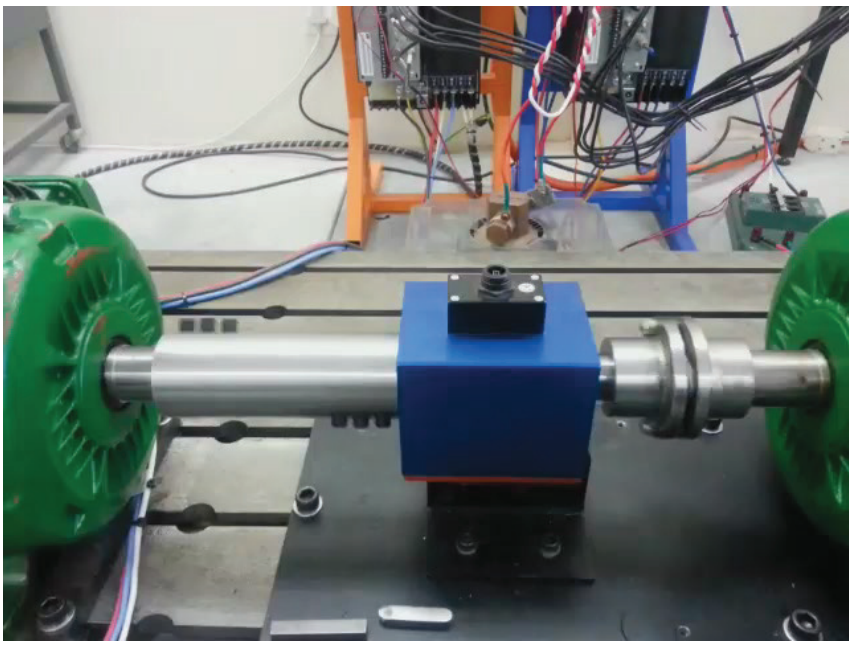

Figure 5.7: Torque sensor with solid and flexible couplings

The decision was made to attach the RSM to the torque sensor by means of a solid coupling, while the IM would still be connected using the flexible coupling, and with the torque sensor effectively floating between the machines (See Fig.5.7). The solid coupling was manufactured by the author to a high degree of accuracy to eliminate any possible oscillations. Testing of the new assembly showed sufficient reduction in vibrations and visible oscillations for testing to continue, with the remaining oscillations attributed to a very slight bend in the shaft of the RSM.

5.4 RSM Measured Performance

5.4.1 Operating Points Estimations

The first task before the final tests can take place is to estimate the magnitude and angle of the current vector for each of the operating points. This is done by generating torque curves for the RSM and using the data to calculate the system efficiency on those curves. The approximate current vectors are then calculated that match the desired load points with the highest system efficiency. This also provides an opportunity to compare the true performance of the machine with the simulation results.

5.4.1.1 Initial Difficulties

Initial attempts at generating torque curves were met with difficulties when it was found that the peaks of the torque curves occur at lower current angles than expected. This can be seen in Fig. 5.8 which shows how the measured torque curve compares to simulations at 1500 rpm. It is evident from Fig. 5.9 and Fig. 5.10 that the shape of the torque curve below 60^o and above 120^o is a result of the RSM's back EMF limiting the supply current.

When considering Fig. 5.9 it becomes apparent that the influence of the endwinding inductance may have been overestimated, because the operable region of the RSM is in fact larger than what the simulations would suggest. However, the figure also exposes an oversight made by the author. The location of the operating point for rated output leaves little room for error with the voltage designed to be as near to 380 V as possible. In retrospect it may have

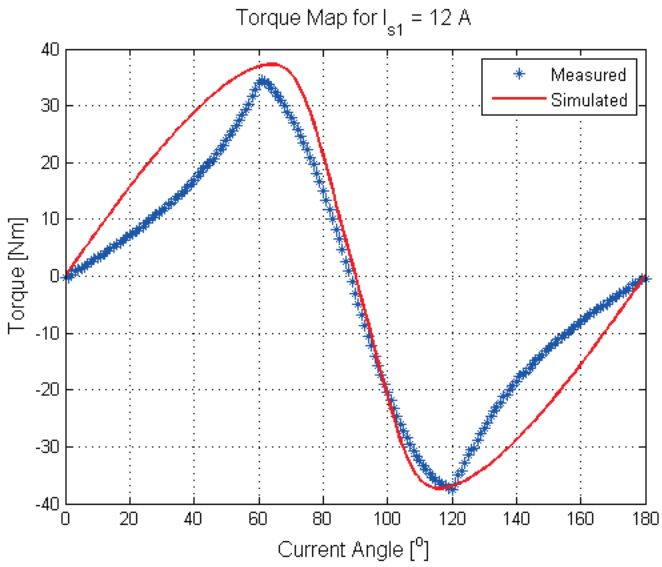

Figure 5.8: Simulated and measured torque versus current angle at 12 A_{rms}.

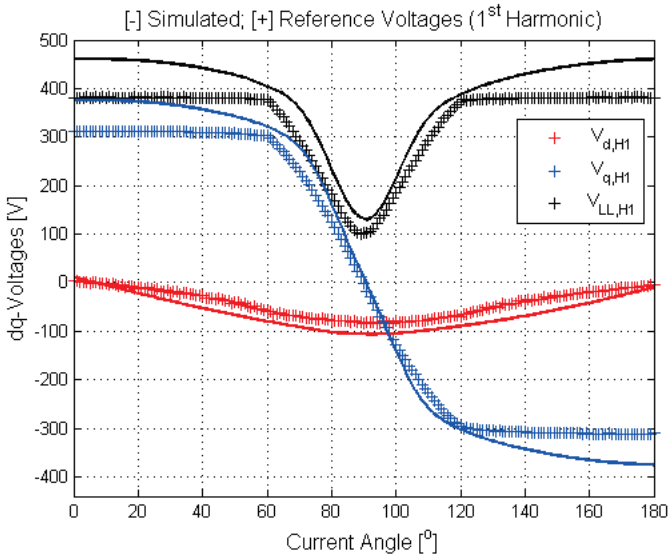

Figure 5.9: Simulated and applied dq-voltages versus current angle at 12 A_{rms}.

been better to design the RSM for a slightly lower rated voltage to avoid such risk, as well as to give the control algorithm more range to operate within.

In order for testing to continue two possible courses of action could be taken. The first would be to still work with the smallest magnitude current vector for which the RSM generates the required torque, while the other option would be to increase the grid voltage to allow the RSM to be operated at a higher rated voltage. The primary concern with the first approach is that the

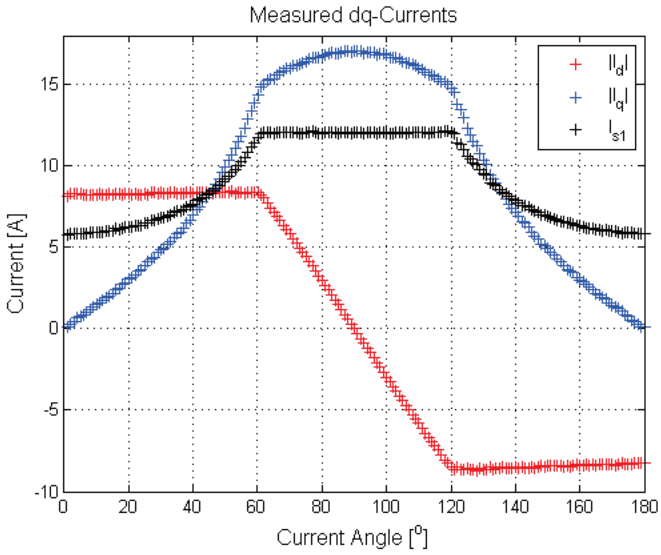

Figure 5.10: Applied dq-currents versus current angle at 12 A_{rms}.

control algorithm may not be stable if the RSM needs to operate at rated voltage, because any deviation of the current angle in either direction would result in sharp changes in developed torque.

Increasing the supply voltage would allow for greater confidence in the control stability, but it would also mean that the RSM would be tested in a way that is closer to how it was intended, albeit for a higher rated voltage. The downside to this approach is that any comparisons made to the IM would be less relevant, because the IM's rated voltage is still limited to 380 V.

Additional tests showed that to generate a torque curve with a smoother gradient around the peaks, the supply would need to be increased just enough for tests to be conducted for a rated voltage that is 10 V higher. This also means the difference in rated voltage between the two machines won't be so great as to make any comparison with the IM pointless, and the IM's inverter would be operating with the same increased grid voltage. Based on these considerations, the decision was made to proceed with the second approach.

5.4.1.2 RSM in motor mode:

With the grid voltage increased, new torque curves are generated for current angles from 45^o up to 80^o. The results are shown in Fig. 5.11 together with the expected torque from simulations. The simulated torque was adjusted downward using measured wind and friction torque loss, which isn't calculated

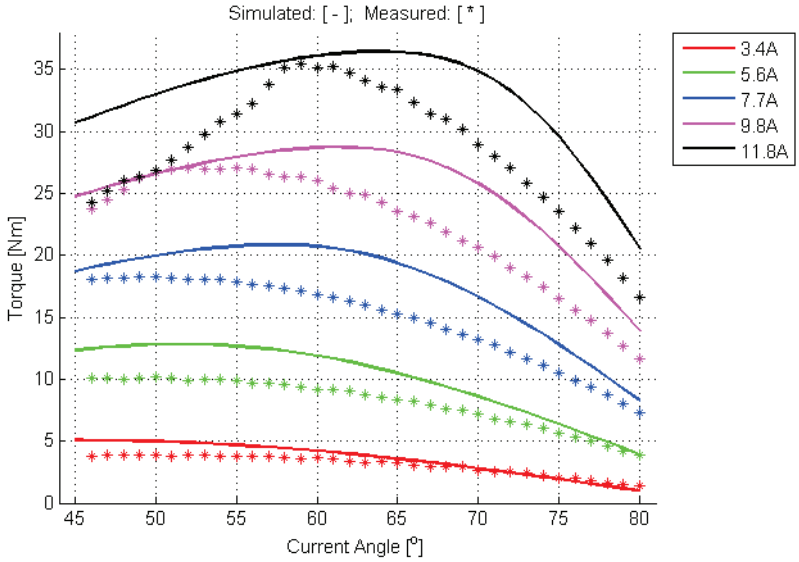

Figure 5.11: Simulated torque compared to measured torque in motor mode.

by the simulation, to make the comparison more fair. These losses were found by simply running the IM at 1500 rpm and taking the average reading from the torque sensor.

The linear behaviour of the measured torque at 12.0 A is once again due to the RSM's back EMF limiting the supply current, meaning the phase current only reaches the desired 12.0 A from 59^o onward. However, the MTPA operating points for all currents are now accessible.

Two things that were already evident from Fig. 5.8 are more visible now in Fig. 5.11 and can be analysed in more detail. Firstly, the peak torque at lower currents is consistently less than what was expected, ranging from 25 % less at 3.5 A to roughly 3 % less at 12.0 A. Secondly, as the current increases, the measured torque reaches its peak at lower current angles than the simulated torque. The discrepancy becomes as large as 9^o at 9.9 A.

The shape of the measured curves indicates that the RSM isn't saturating as was predicted by the simulations. It is unlikely that the problem is caused by the BH-curve used in the simulations, as repeated simulations with various materials didn't produce peak torque at lower current angles. A possible cause may be 3D effects that aren't accounted for by the static 2D simulations. It is also possibly due to damage caused to the ribs of many of the rotor laminations during transportation from the manufacturers, or it may be that the air-gap is larger than the design specified. As an illustration of the effect the air-gap

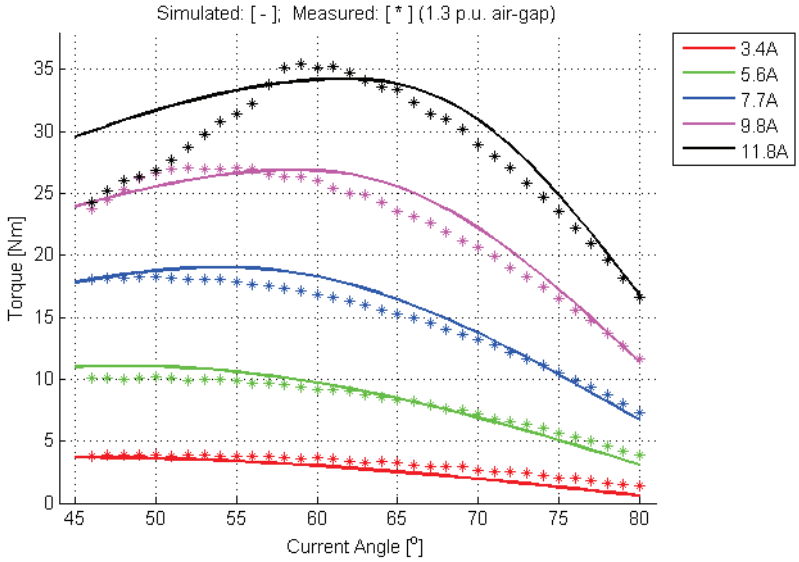

Figure 5.12: Simulated torque compared to measured torque for 1.3 p.u air-gap.

has on the RSM's torque, Fig. 5.12 shows how the simulated torque compares to the measured torque when the air-gap is increased to 1.3 per unit from 0.34 mm to 0.44 mm.

The fitted curves of Fig. 5.13 and Fig. 5.14 are generated from the data using 4^{th} degree polynomial regression. These curves are then used to estimate the operating points by finding the angle for each reference current in Fig. 5.13

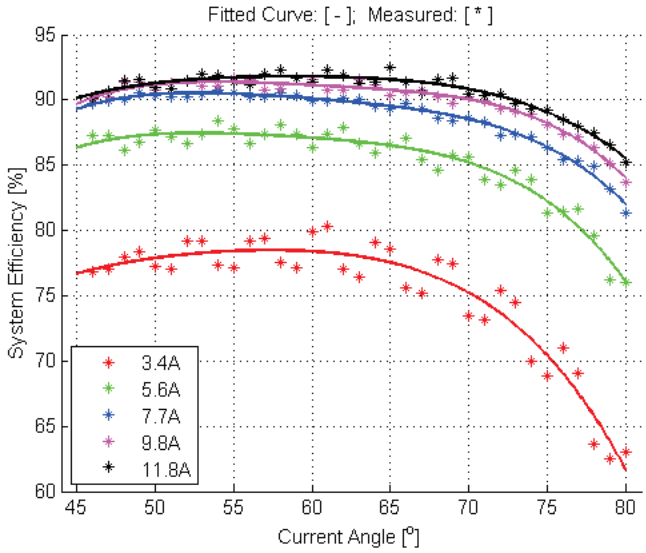

Figure 5.13: RSM system efficiency measured against current angle and magnitude.

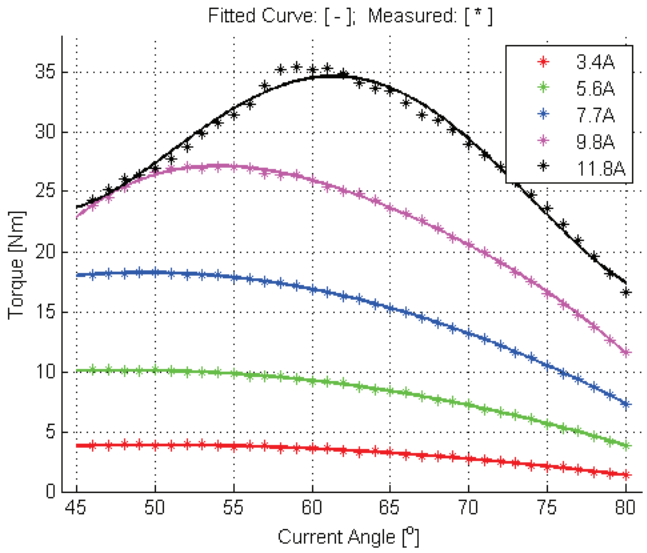

Figure 5.14: RSM Torque measured against current angle and magnitude.

where maximum system efficiency is attained. The corresponding torque is then taken from the data shown in Fig. 5.14. Linear interpolation is used to determine the operating points that produces the desired loads. The author has been unable to identify a cause for the oscillating behaviour of the system efficiencies in Fig. 5.13.

5.4.1.3 RSM in generator mode:

In generator mode the torque curves are generated for the same reference currents as before, but at negative current angles. The measured torque and simulated torque for generator mode are shown in Fig. 5.15.

Three points of comparison can be made between Fig. 5.15 and Fig. 5.11. Firstly, it appears as though the current controller was more stable when the generator mode torque curve measurements were performed and could thus supply more voltage than in motor mode. This resulted in the currents not being limited at lower current angles. Secondly, the RSM is still generating less torque than expected from the simulations, but to a lesser extent than for motor mode. In this case the torque error ranges from 21 % at 3.5 A to 1.3 % at 12 A. Lastly, the current angle where maximum torque is attained also differs by as much as 8^o at higher current references.

When comparing Fig. 5.13 and Fig. 5.16 it is interesting to note that the RSM is less efficient in generator mode than in motor mode. As before, the

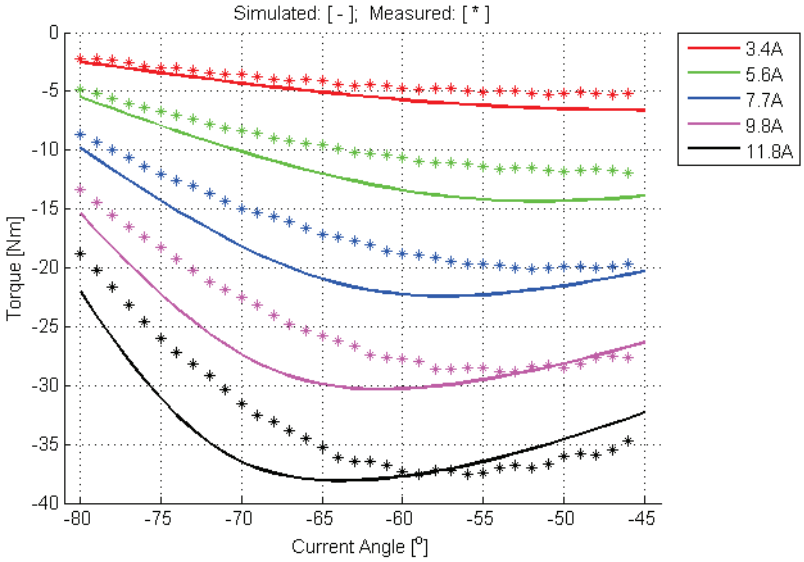

Figure 5.15: Simulated torque compared to measured torque in generator mode.

data represented in Fig. 5.16 and Fig. 5.17 is used to estimate the operating points where the desired load is generated.

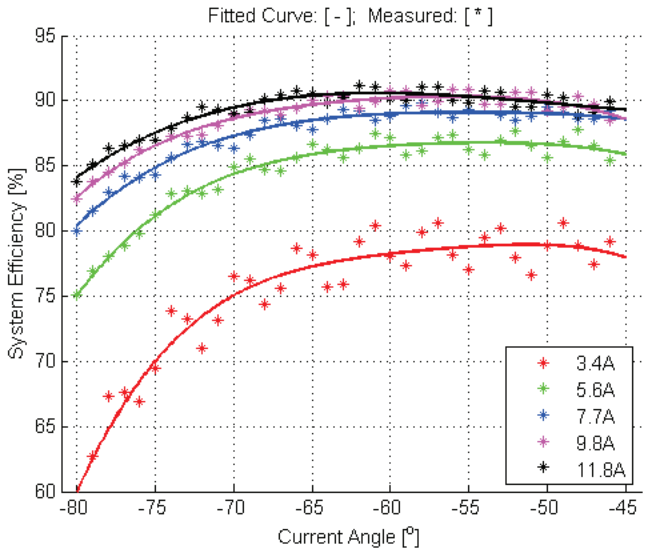

Figure 5.16: RSM system efficiency measured against current angle and magnitude.

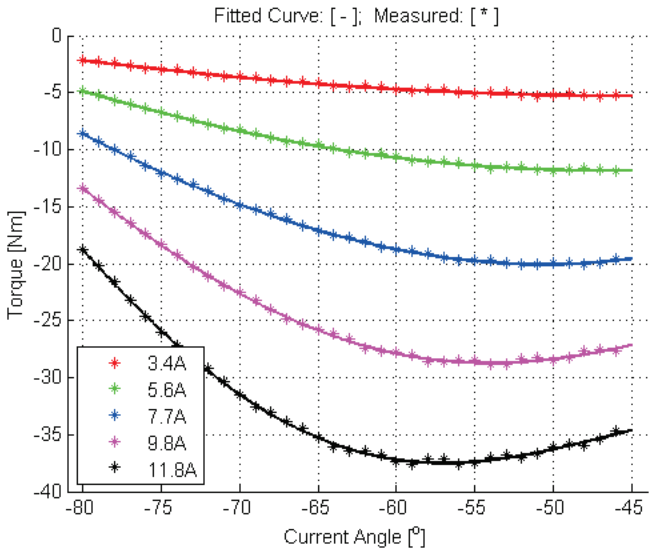

Figure 5.17: RSM Torque measured against current angle and magnitude.

5.4.2 Performance Rating Measurement

With the operating point determined, the final test is performed. An infra-red camera is used to record the frame temperature of the RSM before and after the initial heat run. The frame temperatures are shown in Fig. 5.18(a) and Fig. 5.18(b) respectively. The RSM's frame temperature climbed by 23 ^{o}C over the hour and a half that it took the machine to reach thermal equilibrium. Measurements of the phase resistance before and after the test shows an increase from 0.55 Ω per phase to 0.63 Ω per phase.

After the heat run has been completed the control program is executed and allowed to go through the process of measuring the performance of the RSM at

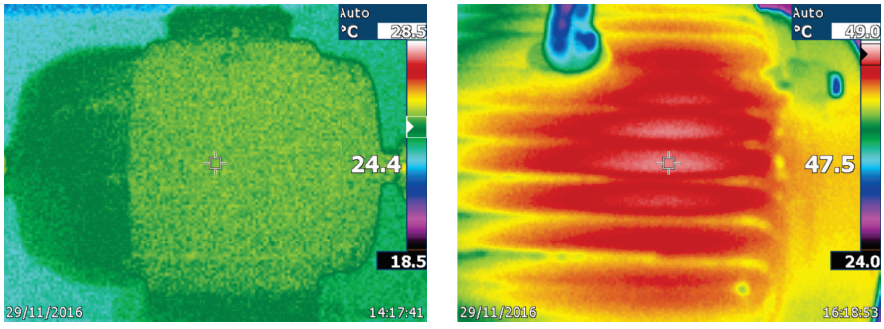

(a) Before Test. (b) Thermal equilibrium.

Figure 5.18: RSM frame temperatures.

Table 5.3: Measured RSM efficiencies

#	Torque	n [rpm]	Motor Eff.	System Eff.
1	35.5 Nm	1500	94.3%	91.4%
2	26.3 Nm	1500	93.9%	90.9%
3	26.3 Nm	1125	90.9%	89.8%
4	17.7 Nm	1125	90.7%	89.1%
5	26.5 Nm	750	88.2%	87.2%
6	9.1 Nm	750	88.2%	85.1%
7	26.8 Nm	375	80.6%	79.0%
Weighted:			89.8%	87.8%

each of the operating points. It acquires 30 seconds of data for each point and returns to full speed/load for 60 seconds after each measurement to maintain thermal equilibrium. The measured efficiencies are given in Table. 5.3 and a more detailed breakdown of the RSM's performance at rated conditions is given in Table 5.4.

The first result that can be taken from Table. 5.4 is the efficiency for the RSM at rated conditions, which is better than what was expected from the results in Table. 5.2. At 94.3 % the motor efficiency is sufficient to guarantee an IE4 efficiency rating for variable speed applications under the currently established limits. The 0.74 power factor at full-load also closely matches the simulated power factor at 59^o current angle.

When comparing the results of Table. 5.3 with that of Table. 4.2 and Table. 5.2 it is interesting to note that the rated efficiency of the RSM agrees more closely to the former. In both cases though the motor efficiency was overestimated significantly for the operating points at lower speeds. This implies that the simulation model still requires a lot of refinement in order to estimate the RSM's efficiency at lower speeds more accurately.

Table 5.4: RSM measured full load performance

Parameter	Value
Rated Power	5.58 kW
Rated Torque	35.5 Nm
Power Factor	0.74
Rated Voltage	390 V
Rated Current	11.9 A
Current Density	4.68 A/mm^2
Current Angle	59.0^o
Copper Losses	268 W
Other Losses	69 W
Motor Efficiency	94.3%
Drive System Efficiency	91.4%

Table 5.5: Measured IM efficiencies

#	Torque	n [rpm]	Motor Eff.	System Eff.
1	35.1 Nm	1500	84.5%	83.1%
2	26.3 Nm	1500	84.7%	82.9%
3	26.2 Nm	1125	81.8%	80.6%
4	17.3 Nm	1125	80.3%	78.8%
5	26.0 Nm	750	78.3%	76.7%
6	8.2 Nm	750	70.4%	65.4%
7	25.7 Nm	375	68.2%	64.9%
Weighted:			78.5%	76.3%

5.5 Measured Induction Machine Performance and Comparison

The testing procedure applied to the RSM is now repeated for the IM, which needed two hours to reach thermal equilibrium. During this time the frame temperature climbed by 39.3 ^{o}C and the per-phase resistance went from 0.77 Ω at 23.5^{o}C to 0.93 Ω at 62.8 ^{o}C. The results are given in Table. 5.5.

The first conclusion that can be drawn from the data of Table. 5.5 is that the RSM achieved much better efficiency levels and hence maintained its efficiency advantage over the IM. The IM's weighted motor efficiency is 78.5 % compared to the RSM at 89.8 %, and the system efficiency is 76.3 % against the RSM's 87.8 %, which makes the RSM the better choice for variable speed and torque applications. The RSM's superior system efficiency of 91.4 % against the IM's 83.1 % at rated conditions means that, at the given power level, the RSM is the better option for single speed applications as well.

The efficiency de-rating of the IM from the nameplate value of 89.6 % to 84.5 %, at full load, is to be expected when driving the IM with a VSD. This means however that the IM would only receive an IE2 classification for VSD applications. The measured power factor at full-load is 0.862 which is reasonably close to the nameplate value of 0.87, considering the fact that the full load test was run at 1500 rpm instead of the rated 1460 rpm. While it would be possible to increase the efficiency of the IM by using flux vector control, or optimum V/Hz ratios, it is unlikely that the difference would be enough to out-perform the RSM.

Chapter 6

Conclusions and Recommendations

6.1 Conclusions

A clear answer to the research question has been found. As expected at the power range of 5.5 kW, the RSM system outperformed the IM system in terms of total efficiency at every operating point tested. The RSM is thus a better choice for variable speed and torque applications, especially where a duty profile with a wide operating range is anticipated.

The RSM performed much better at rated conditions than was expected from the simulations, but also significantly worse than expected at lower speeds. This means that during post-processing the losses were overestimated at rated conditions, but underestimated at lower speeds. Thus, the RSM model requires refinement in the way it calculates losses in order for the RSM's performance to be predicted more accurately.

It was noticed during the optimisation process that the inclusion of inverter losses led to an indirect optimisation of the power factor. It should be said, however, that the same would happen if the objective was to obtain maximum torque per ampere at this power level. It might still be useful to include the inverter losses in the optimisation if material minimisation was the objective while using minimum system efficiency as a constraint to match a desired efficiency class.

6.2 Recommendations for Future Studies

The following recommendations for future research can be made:

- In the future it would be advantageous to design the RSM for a slightly lower rated voltage. This will allow for a more stable control algorithm that isn't limited by DC-link as much. A possible drawback to this would be increased losses in the frequency converter, although the extent of the drawback could be the topic of another study.
- It would make a valuable contribution to the body of knowledge around RSMs if a study (or more likely a series of studies) could be made of the stray load losses of the RSM. It would be of significant use to researchers and developers if a formula akin to the assigned stray losses for the IM could be created.
- Efforts should be made to develop a better model of the RSM that could be used to more accurately predict the efficiency or losses over an entire operating range. This would ideally follow after (or be part of) the previously stated recommended research. The improved model will then be usable as part of an optimisation procedure that generates a design with the duty profile of the application accounted for.
- While it is known that the RSM maintains its efficiency advantage over the IM only up to around 300 kW, it is uncertain at which point the efficiency of the IM would surpass that of a RSM Power Drive System. If this feasible power range could be established more clearly it would be of use to all interested stakeholders. It could be expected that this would be difficult as the range would likely depend on the intended application.

Appendices

Appendix A

Lamination Technical Drawings

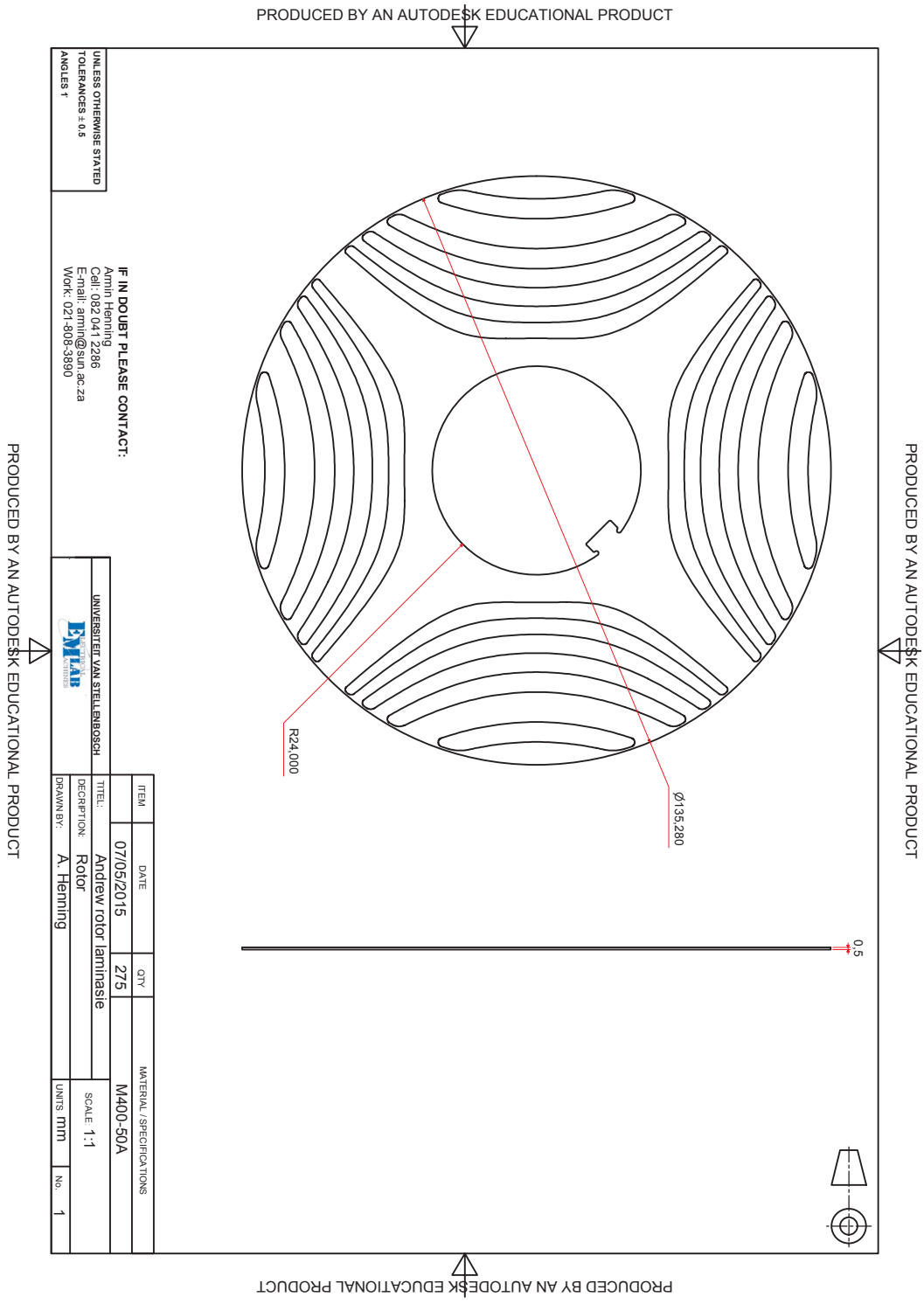

Figure A.1: Rotor technical drawing

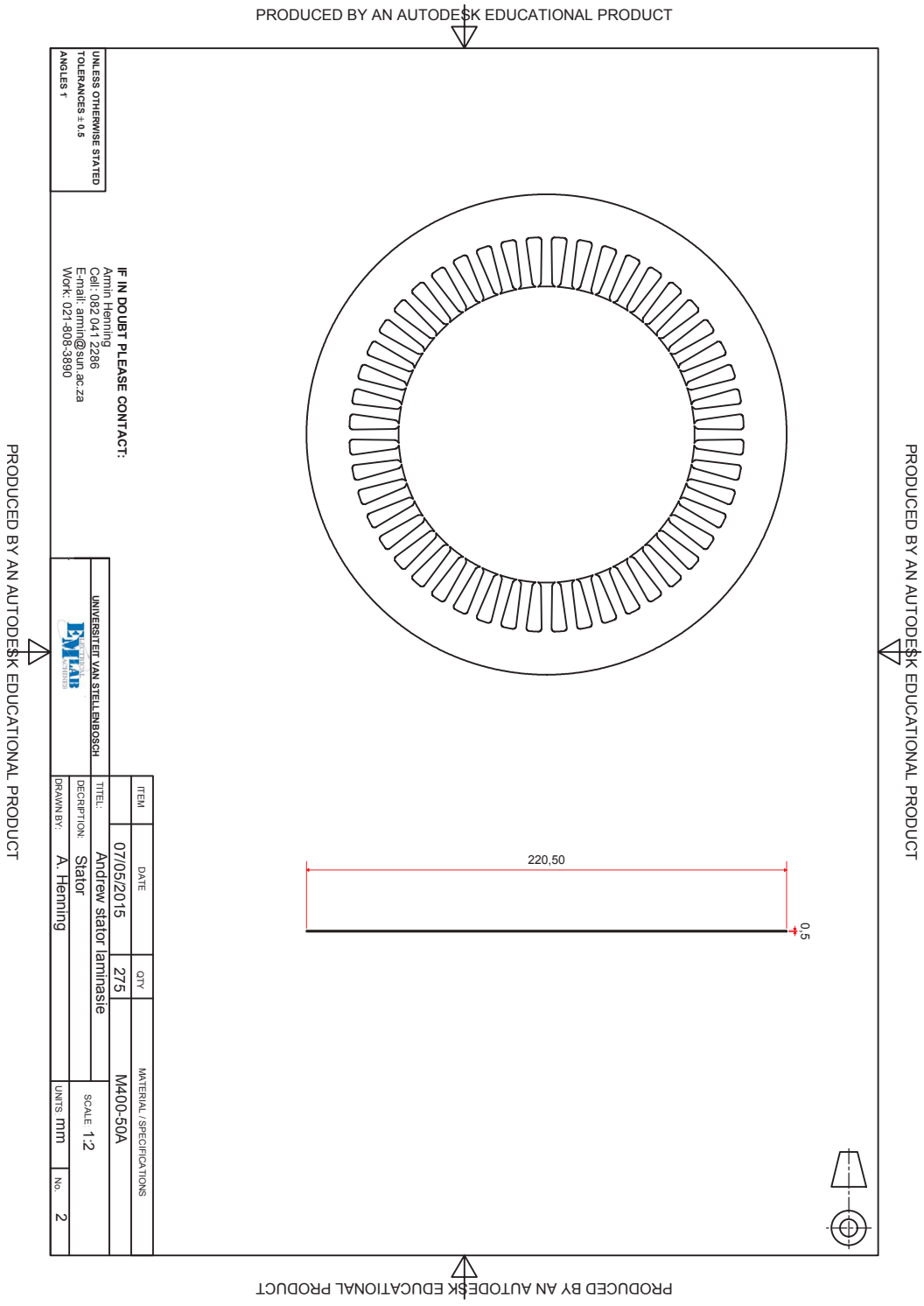

Figure A.2: Stator technical drawing

Bibliography

[1] Malinowski, J., Hoyt, W., Zwanziger, P. and Finley, B.: Motor and Drive-System Efficiency Regulations: Review of Regulations in the United States and Europe. *IEEE Industry Applications Magazine*, vol. 23, no. 1, pp. 34–41, Jan 2017. ISSN 1077-2618. Available at `http://ieeexplore.ieee.org`.

[2] Rooks, J.A. and Wallace, A.K.: Energy efficiency of variable speed drive systems. In: *Conference Record of the 2003 Annual Pulp and Paper Industry Technical Conference, 2003.*, pp. 160–163. June 2003. ISSN 0190-2172.

[3] Vagati, A.: The synchronous reluctance solution: a new alternative in AC drives. In: *Industrial Electronics, Control and Instrumentation, 1994. IECON '94., 20th International Conference on*, vol. 1, pp. 1–13 vol.1. Sep 1994.

[4] Palmieri, M., Perta, M., Cupertino, F. and Pellegrino, G.: Effect of the numbers of slots and barriers on the optimal design of synchronous reluctance machines. In: *Optimization of Electrical and Electronic Equipment (OPTIM), 2014 International Conference on*, pp. 260–267. May 2014.

[5] Gamba, M., Pellegrino, G. and Cupertino, F.: Optimal number of rotor parameters for the automatic design of synchronous reluctance machines. In: *2014 International Conference on Electrical Machines (ICEM)*, pp. 1334–1340. Sept 2014.

[6] Howard, E., Kamper, M.J. and Gerber, S.: Asymmetric flux barrier and skew design optimization of reluctance synchronous machines. *IEEE Transactions on Industry Applications*, vol. 51, no. 5, pp. 3751–3760, Sept 2015. ISSN 0093-9994.

[7] Department of Energy: Integrated Energy Plan. GN 1430 in *Government Gazette* No. 40445, pp. 15-207, 25 Nov 2016. South Africa.

[8] Department of Energy: Post-2015 National Energy Efficiency Strategy. GN 948 in *Government Gazette* No. 40515, pp. 426-471, 23 Dec 2016. South Africa.

[9] Doppelbauer, M.: Current developments in iec standards for energy efficiency of electric motors and for IECEE global motor energy efficiency (GMEE) program. In: *Energy Efficiency in Motor Driven Systems, Proceedings of the 8th International Conference EEMODS'2013*, pp. 807–815. October 2013. Available at `http://publications.jrc.ec.europa.eu/repository/handle/JRC90351`.

[10] Doppelbauer, M.: Update on IEC motor and converter standards. In: *Proceedings of the 6th international Motor Summit for energy efficient motor systems*, pp. 24–25. October 2016. Zurich, Switzerland.

[11] Tsoumas, I.P., Tischmacher, H. and Kollensperger, P.: The European Standard EN 50598-2: Efficiency classes of converters and drive systems. In: *2014 International Conference on Electrical Machines (ICEM)*, pp. 929–935. Sept 2014.

[12] Lipo, T.A.: Synchronous reluctance machines - a viable alternative for AC drives? *Electric Machines and Power Systems*, vol. 19, no. 6, pp. 659–671, Nov-Dec 1991. Available Online at `http://lipo.ece.wisc.edu/`; Last seen: 20 July 2017.

[13] Vagati, A., Fratta, A., Franceschini, G. and Rosso, P.M.: AC motors for high-performance drives: a design-based comparison. In: *Industry Applications Conference, 1995. Thirtieth IAS Annual Meeting, IAS '95., Conference Record of the 1995 IEEE*, vol. 1, pp. 725–733 vol.1. Oct 1995. ISSN 0197-2618.

[14] Boglietti, A., Cavagnino, A., Pastorelli, M. and Vagati, A.: Experimental comparison of induction and synchronous reluctance motors performance. In: *Fourtieth IAS Annual Meeting. Conference Record of the 2005 Industry Applications Conference, 2005.*, pp. 474–479 Vol. 1. Oct 2005. ISSN 0197-2618.

[15] Vagati, A., Pastorelli, M., Francheschini, G. and Petrache, S.C.: Design of low-torque-ripple synchronous reluctance motors. *IEEE Transactions on Industry Applications*, vol. 34, no. 4, pp. 758–765, Jul 1998. ISSN 0093-9994.

[16] Bomela, X.B. and Kamper, M.J.: Effect of stator chording and rotor skewing on performance of reluctance synchronous machine. *IEEE Transactions on Industry Applications*, vol. 38, no. 1, pp. 91–100, Jan 2002. ISSN 0093-9994.

[17] Landsmann, P., Kennel, R., de Kock, H.W. and Kamper, M.J.: Fundamental saliency based encoderless control for reluctance synchronous machines. In: *The XIX International Conference on Electrical Machines - ICEM 2010*, pp. 1–7. Sept 2010.

[18] Consoli, A., Scarcella, G., Scelba, G., Testa, A. and Triolo, D.A.: Sensorless rotor position estimation in synchronous reluctance motors exploiting a flux deviation approach. *IEEE Transactions on Industry Applications*, vol. 43, no. 5, pp. 1266–1273, Sept 2007. ISSN 0093-9994.

[19] Schroedl, M.: Sensorless control of ac machines at low speed and standstill based on the ldquo;inform rdquo; method. In: *Industry Applications Conference, 1996. Thirty-First IAS Annual Meeting, IAS '96., Conference Record of the 1996 IEEE*, vol. 1, pp. 270–277 vol.1. Oct 1996. ISSN 0197-2618.

[20] Landsmann, P., Paulus, D., Stolze, P. and Kennel, R.: Saliency based encoderless predictive torque control without signal injection for a reluctance synchronous machine. In: *Proceedings of 14th International Power Electronics and Motion Control Conference EPE-PEMC 2010*, pp. S1–10–S1–17. Sept 2010.

[21] ABB: Low voltage IE4 synchronous reluctance motors. August 2016. Available online at: `http://new.abb.com/`, Last seen: 11/09/2017.

[22] SIEMENS AG: Small step, big impact: Energy efficiency and dynamic performance. 2016. Available online at: `http://siemens.com/`, Last seen: 11/09/2017.

[23] Germishuizen, J.J., der Merwe, F.S.V., der Westhuizen, K.V. and Kamper, M.J.: Performance comparison of reluctance synchronous and induction traction drives for electrical multiple units. In: *Conference Record of the 2000 IEEE Industry Applications Conference. Thirty-Fifth IAS Annual Meeting and World Conference on Industrial Applications of Electrical Energy (Cat. No.00CH37129)*, pp. 316–323 vol.1. 2000. ISSN 0197-2618.

[24] Villet, W.T. and Kamper, M.J.: Variable-gear EV reluctance synchronous motor drives - an evaluation of rotor structures for position-sensorless control. *IEEE Transactions on Industrial Electronics*, vol. 61, no. 10, pp. 5732–5740, Oct 2014. ISSN 0278-0046.

[25] Kamper, M.: *Design Optimisation of cageless flux barrier rotor reluctance synchronous machine*. Ph.D. thesis, University of Stellenbosch, 1996.

[26] IEC 60034-2-1:2014: Rotating Electrical Machines – Part 2–1: Standard Methods for Determining losses & Efficiency from Tests. Standard, International Electrotechnical Commission, Geneva, CH, June 2014.

[27] IEC TS 60034-2-3:2013: Rotating electrical machines – Part 2–3: Specific test methods for determining losses and efficiency of converter-fed induction motors. standard, International Electrotechnical Commission, Geneva, CH, November 2013.

[28] Wolf, M., d. T. Mouton, H., van der Merwe, J.W. and Koeslag, F.: An investigation of switching and conduction losses in inverters under varying inductor ripple current. In: *AFRICON 2009*, pp. 1–6. Sept 2009. ISSN 2153-0025.